



1

2 **Sensitivity of the WRF-Chem v4.4 ozone, formaldehyde, and precursor**
3 **simulations to multiple bottom-up emission inventories over East Asia during the**
4 **KORUS-AQ 2016 field campaign**

5

6 Kyoung-Min Kim¹, Si-Wan Kim^{2*}, Seunghwan Seo¹, Donald R. Blake³, Seogju Cho⁴,
7 James H. Crawford⁵, Louisa Emmons⁶, Alan Fried⁷, Jay R. Herman^{8,9}, Jinkyu Hong¹,
8 Jinsang Jung¹⁰, Gabriele Pfister⁶, Andrew J. Weinheimer⁶, Jung-Hun Woo¹¹, and Qiang
9 Zhang¹²

10

11 ¹Department of Atmospheric Sciences, Yonsei University, Seoul, South Korea

12 ²Irreversible Climate Change Research Center, Yonsei University, Seoul, South Korea

13 ³Department of Chemistry, University of California at Irvine, Irvine, CA, US

14 ⁴Seoul Metropolitan Government Research Institute of Public Health and
15 Environment, Gyeonggi-do, South Korea

16 ⁵NASA Langley Research Center, Hampton, VA, US

17 ⁶National Center for Atmospheric Research, Boulder, CO, US

18 ⁷Institute of Arctic and Alpine Research, University of Colorado, Boulder, CO, US

19 ⁸NASA Goddard Space Flight Center, Greenbelt, MD, US

20 ⁹University of Maryland Baltimore County, Baltimore, MD, USA

21 ¹⁰Korea Research Institute of Standards and Science, Daejeon, South Korea

22 ¹¹Department of Advanced Technology Fusion, Konkuk University, Seoul, South
23 Korea

24 ¹²Department of Earth System Science, Tsinghua University, Beijing, China

25

26

27 *To whom correspondence should be addressed. E-mail: siwan.kim@yonsei.ac.kr

28

29 Date: 6/21/2023



1 **Abstract**

2 In this study, the WRF-Chem v4.4 model was utilized to evaluate three bottom-up
3 emission inventories (EDGAR-HTAP v2, v3, and KORUS v5) using surface and
4 aircraft data in East Asia during the Korea-United States Air Quality (KORUS-AQ)
5 campaign period in 2016. All emission inventories were found to reproduce the diurnal
6 variations of O₃ and NO₂ as compared to the surface monitor data. However, the spatial
7 distributions of the daily maximum 8-hour average (MDA8) O₃ in the model do not
8 completely align with the observations. The model MDA8 O₃ had a negative (positive)
9 bias north (south) of 30°N over China. All simulations underestimated the observed CO
10 by 50-60% over China and South Korea. In the Seoul Metropolitan Area (SMA),
11 EDGAR-HTAP v2, v3, and KORUS v5 simulated the vertical shapes and diurnal
12 patterns of O₃ and other precursors effectively, but the model underestimated the
13 observed O₃, CO and HCHO concentrations. Notably, the model aromatic VOCs were
14 significantly underestimated with the three bottom-up emission inventories, although
15 the KORUS v5 shows improvements. The model isoprene estimations had a positive
16 bias relative to the observations, suggesting that the Model of Emissions of Gases and
17 Aerosols from Nature (MEGAN) version 2.04 overestimated isoprene emissions.
18 Additional model simulations were conducted by doubling CO and VOC emissions
19 over China and South Korea to investigate the causes of the model O₃ biases and the
20 effects of the long-range transport on the O₃ over South Korea. The doubled CO and
21 VOC emission simulations improved the model O₃ simulations for the local emission
22 dominant case, but led to the model O₃ overestimations for the transport dominant case,
23 which emphasizes the need for accurate representations of the local VOC emissions
24 over South Korea.



1 1. Introduction

2 Air pollutants not only harm human health but also affect radiative balance, resulting
3 in climate change (Anenberg et al., 2018; Franklin et al., 2015; Lee et al., 2014;
4 Manning and von Tiedemann, 1995; Rosenzweig et al., 2008; Wild et al., 2001).
5 Anthropogenic activities are the primary source of air pollutant emissions, which have
6 significant temporal and spatial variability. Chemical transport models (CTMs) use
7 bottom-up emission data to simulate ambient concentrations of air pollutants. CTMs
8 then process these emissions, tracking their impact through chemistry, transport, and
9 loss through deposition (Zhong et al., 2016). Therefore, sensitivity evaluations of CTMs
10 to anthropogenic emission data are an essential part of atmospheric modeling research.

11 Several bottom-up emission inventories are available for chemical modeling of
12 Asia, including the Multi-resolution Emission Inventory for China (MEIC), Regional
13 Emission inventory in Asia (REAS), and Emissions Database for Global Atmospheric
14 Research-Hemispheric Transport of Air Pollution (EDGAR-HTAP). Since 2010,
15 Tsinghua University has developed the high-resolution MEIC emission inventory for
16 China and updated the data to the v1.3, providing anthropogenic emissions by sector
17 and species from 2008 to 2017 (Zheng et al., 2018). REAS provides emission data in
18 Asia from 1950 to 2015 (Kurokawa and Ohara, 2020). In Europe, EDGAR-HTAP has
19 been developed and widely used for CTM simulations from global to regional scale
20 (Kim et al., 2021; Sharma et al., 2017; Sicard et al., 2021). Recently, EDGAR-HTAP
21 v3 has been published, covering 19 years from 2000 to 2018 compared to only two
22 years (2008 and 2010) in the version 2 data (Crippa et al., 2023). Zhong et al. (2016)
23 compared REAS with EDGAR in July, 2007 over China, while Saikawa et al. (2017)
24 compared 5 emission inventories including REAS, EDGAR, MEIC in China, without



1 validation. As bottom-up emission inventories are continuously updated for recent years,
2 there is an ongoing need to evaluate new emissions data.

3 The Ministry of Environment (MOE) in South Korea and National Aeronautics and
4 Space Administration (NASA) in the U.S. conducted the Korea-United States Air
5 Quality (KORUS-AQ) campaign in May-June 2016. The campaign provided a variety
6 of data sets, including ground-based and airborne observations, useful for the validation
7 of model simulations. The KORUS emissions, developed by Konkuk University, were
8 used by many modeling teams to simulate the air pollutant concentrations during the
9 campaign period. In this study, we selected the EDGAR-HTAP versions 2, v3, and
10 KORUS version 5 emission data and used the Weather Research and Forecasting model
11 coupled with Chemistry (WRF-Chem) version 4.4 for intercomparison of the three
12 emissions data sets. O₃ and its major precursors were selected for model evaluation and
13 the model results were validated with surface observation data in China and South
14 Korea and aircraft data acquired over the South Korean peninsula and surrounding
15 waters.

16

17 **2. Data and Methods**

18 **2.1. WRF-Chem model configurations**

19 In this study, we utilized the WRF-Chem v4.4, which was developed by the National
20 Oceanic and Atmospheric Administration (NOAA) and National Center for
21 Atmospheric Research (NCAR), to simulate meteorological variables and chemical
22 species in the atmosphere (Grell et al., 2005). The WRF-Chem v4.4 includes N₂O₅
23 heterogeneous chemistry that consists of several chemical reactions related with ClNO₂



1 and N_2O_5 reactions, resulting in nitrate aerosol. The reactions are incorporated in
2 Secondary Organic Aerosol-Volatility Basis Set (SOA-VBS) with Regional
3 Atmospheric Chemistry Mechanism (RACM) chemistry option (chem = 108) in WRF-
4 Chem (Li et al., 2016).

5 We set 59 vertically customized eta (η) levels as vertical layers. The model's first
6 layer height is approximately 40 m above ground level for the entire domain. The
7 model's vertical layers are designed to include about 17 layers under 1.5 km to simulate
8 planetary boundary layer chemistry and near surface vertical distribution in detail. The
9 horizontal resolution is $28 \times 28 \text{ km}^2$. The simulations in this study start at 12 UTC on
10 April 24 and end at 12 UTC on June 11. The model meteorology restarts every 12 UTC
11 (9 PM local time in South Korea) to minimize numerical errors. After the first 7 days
12 of model initiation (spin-up), we analyzed the model results from May 1 to June 10. We
13 used China standard time (+8 UTC) and Korea standard time (+9 UTC) for evaluations
14 with observations. The model physics, chemistry, and aerosol schemes are summarized
15 in Table S1 with corresponding references. The Global Forecast System (GFS) Final
16 (FNL) analysis data are used for meteorological input and boundary conditions. The
17 Community Atmosphere Model with Chemistry (CAM-Chem) output is used for
18 chemical boundary conditions (<https://www.acom.ucar.edu/cam-chem/cam-chem.html>)
19 (Buchholz et al., 2019; Emmons et al., 2020). We used the Model of Emissions of Gases
20 and Aerosols from Nature (MEGAN) v2.04 to calculate biogenic emissions (Guenther
21 et al., 2006). We did not account for fire emissions because of small impact on air
22 quality simulations during the KORUS-AQ campaign period (Park et al., 2021).



1 2.2. The model simulations using different anthropogenic emissions

2 2.2.1. Bottom-up emission data

3 EDGAR-HTAP v2, v3, and KORUS v5 emissions are compared with respect to their
4 spatial distribution and total amount in Figure 1 and Table S3. We applied the same
5 diurnal factor for all three emissions data by species, following the diurnal patterns for
6 the Los Angeles Basin as in Kim et al. (2016) (also see Figure S1).

7 EDGAR-HTAP v2 provides 2-dimensional emissions of CH₄, CO, SO₂, NO_x (NO
8 + NO₂), non-methane volatile organic compound (NMVOC), NH₃, PM₁₀, PM_{2.5}, BC,
9 and OC in 2008 and 2010 with a horizontal resolution of 0.1° x 0.1°. We used 2010 data
10 since it is the most recent data available. The data are partitioned by each sector and its
11 sources such as air, ships, energy, industry, transport, residential, and agriculture
12 (https://edgar.jrc.ec.europa.eu/dataset_htap_v2). For East Asia, it included data from
13 the Model Inter-Comparison Study for Asia (MICS-Asia) and REAS v2.1. In South
14 Korea, it adopted data from the Clean Air Policy Support System (CAPSS) (Janssens-
15 Maenhout et al., 2015), and the underlying emission data had an original horizontal
16 resolution of 0.25° x 0.25° over East Asia, which is resampled to 0.1° x 0.1° resolution
17 by raster resampling and aggregation. The specifically mapped EDGAR-HTAP v2 data
18 were obtained through the WRF-Chem site (<https://www.acom.ucar.edu/wrf-chem/download.shtml>) in the *anthro_emiss* program with the Model for Ozone and
19 Related chemical Tracers (MOZART) species. The *anthro_emiss* program converts the
20 EDGAR-HTAP v2 data into 28 x 28 km² grid by the RACM chemical species. It
21 mapped the MOZART volatile organic compounds (VOC) species into the RACM
22 VOC species (See the detailed equations in Supporting Information, Table S4) (Li et al.,
23 2014; Emmons et al., 2010).



1 The EDGAR-HTAP v3 is extended to much longer time scale than the previous
2 version EDGAR-HTAP (v2). The EDGAR-HTAP v3 covers 2000 to 2018 with a more
3 detailed horizontal resolution (https://edgar.jrc.ec.europa.eu/dataset_htap_v3) (Crippa
4 et al. 2023). While EDGAR-HTAP v2 uses MICS-Asia, only the REAS data are used
5 in China and India in the EDGAR-HTAP v3. It adopts the CAPSS-Konkuk University
6 (CAPSS-KU) data for South Korea and emission data provided by the Japanese
7 government for Japan. We chose the data for 2016, according to the KORUS-AQ
8 campaign period. Because the original EDGAR-HTAP v3 data provide VOC as total
9 NMVOC with the unit of ton/month, we distributed the total NMVOC to MOZART
10 VOC species with the ratio of each VOC species to total NMVOC from EDGAR-HTAP
11 v2 in *anthro_emiss* program. Then, the assigned EDGAR-HTAP v3 data were again
12 converted to the RACM.

13 The KORUS v5 emission data represent 2016 in China and 2015 in other regions.
14 The Comprehensive Regional Emissions Inventory for Atmospheric Transport
15 Experiment (CREATE) v2.3 data from 2015 were used and the ship emissions from
16 CAPSS were added near the coastal region in South Korea (Jang et al., 2020; Woo et
17 al., 2012). The CREATE is originally developed by combining REAS, MEIC, Japan
18 Auto-Oil Program emission inventory (JATOP), and Korean Clear Air Policy Support
19 System (CAPSS). The NMVOC species from KORUS v5 were mapped following the
20 Statewide Air Pollution Research Center (SAPRC-99) mechanism, and we also
21 assigned the SAPRC-99 species to RACM (Carter, 2000) (Supporting information,
22 Table S4).

23 Figure 1 shows the spatial distribution of NO, CO, and toluene emissions in May
24 for each inventory. The NO_x emissions were assumed to be emitted as NO. The major



1 cities in China and South Korea had relatively high NO_x, CO, and TOL (toluene and less
2 aromatics defined in RACM, see Table S2) emissions, which are major precursors
3 affecting O₃ formation. We define three boxes representing Eastern China, South Korea,
4 and the Seoul metropolitan area (SMA) and calculated the emissions (see Table S3). In
5 South Korea including SMA, EDGAR-HTAP v3 had the largest NO_x emission among
6 the emission inventories. The KORUS v5 has lower NO_x emissions in Eastern China
7 by 46% and 39% compared to EDGAR-HTAP v2 and v3, respectively. The CO
8 emission was the lowest in EDGAR-HTAP v2 in South Korea, being 56% (69%) lower
9 than that in KORUS v5 (EDGAR-HTAP v3). KORUS v5 showed the highest CO
10 emissions in SMA though EDGAR-HTAP v3 showed more CO emissions in South
11 Korea. However, KORUS v5 had the smallest CO emissions in China, being 7% (9%)
12 lower than that in EDGAR-HTAP v2 (v3). The TOL emission from KORUS v5 is higher
13 than those from EDGAR-HTAP v2 (EDGAR-HTAP v3) by 176% (98%) in China. The
14 relative difference between KORUS v5 and EDGAR-HTAP v2 (EDGAR-HTAP v3) is
15 larger in South Korea by 263%. These discrepancies of VOC emissions may lead to a
16 change in the NO_x/VOC-sensitive regime and O₃ production efficiency. The sensitivity
17 of O₃ formation to NO_x emission has discrepancies by its regime, which will be further
18 discussed in section 3.2.

19

20 **2.2.2. The model experiments**

21 The model experiments are summarized in Table 1. The simulations using EDGAR-
22 HTAP v2, v3, and KORUS v5 emissions are named as EDV2, EDV3, and KOV5,
23 respectively. In this study, we found consistent underestimation of CO and VOC for all



1 emissions by -40% ($\pm 2\%$) and -25% ($\pm 1\%$) (HCHO) compared to DC-8 in South
2 Korea. This is in line with the results reported by Park et al. (2021), who found that
3 almost every model underestimated CO. Underestimation of CO in East Asia is a well-
4 known feature revealed by many studies. For example, Gaubert et al. (2020) mentioned
5 that CAM-Chem underestimates CO during the KORUS-AQ campaign period and
6 presented a CO compensation method utilizing data assimilation with CO observations.
7 Wada et al. (2012) pointed out that EDGAR v4.1 underestimates anthropogenic CO
8 emissions in China by 45% compared to observation-based estimations of CO
9 emissions. Moreover, underestimation of VOC is also found for all anthropogenic
10 emission inventories. Kwon et al. (2021) estimated top-down emissions of
11 anthropogenic VOCs utilizing Geostationary Trace gas and Aerosol Sensor
12 Optimization spectrometer (GeoTASO). They found that top-down VOC emissions
13 were up to 6.9 times higher than bottom-up emissions (KORUS v5). With all emission,
14 O₃ is underestimated at most ground-based observation sites in South Korea. Therefore,
15 we conducted two additional model simulations using EDGAR-HTAP v3 that shows
16 lowest bias of O₃ concentrations compared to DC-8 (-14.2 ppb) than EDGAR-HTAP
17 v2 (-16.9 ppb) and KORUS v5 (-18.1 ppb) over the SMA: one is with twice the
18 anthropogenic CO and VOC emissions in China (EDV3_Ch2) and the other simulation
19 uses double CO and VOC emissions in both China and South Korea (EDV3_ChKo2)
20 to investigate possible improvements in the simulated O₃ and CO from these emission
21 changes.

22



1 **2.3. Observations**

2 **2.3.1. Meteorological data**

3 The meteorological field that WRF-Chem reproduced is validated with the surface
4 synoptic observation (SYNOP) data operated by the World Meteorological
5 Organization (WMO) (<http://www.meteomanz.com>). Surface temperature, relative
6 humidity, and surface wind speed are adopted for model validation. As the SYNOP data
7 are provided every 3 or 6-hourly, we selected model data when the observation data are
8 available. There were 271 sites in China-Taiwan-Hongkong and 48 sites in South Korea.

9

10 **2.3.2. Ground-based observations**

11 The surface observation network used in this study was obtained from Airkorea in South
12 Korea and the China Ministry of Ecology and Environment (MEE) in China. The
13 Airkorea observation network provides 1-hourly measurements of NO₂, SO₂, CO, O₃,
14 PM₁₀, and PM_{2.5} at suburban, background, roadside, city, and port sites
15 (www.airkorea.or.kr). The concentrations of NO₂, CO, and O₃ are measured using the
16 chemiluminescent, non-dispersive infrared, and ultraviolet photometric methods,
17 respectively. The model data with 28 x 28 km² horizontal resolution were linearly
18 interpolated to the 365 sites in South Korea, and we selected NO₂, O₃, and CO for model
19 validation. The Chinese observations were provided by MEE through the website
20 (beijingair.sinaapp.com). Surface NO₂ over China was measured using a molybdenum
21 converter, which has the potential for positive biases due to other NO₂-related oxidation
22 products (Dunlea et al., 2007). In South Korea, the positive biases exist regarding NO₂
23 surface observations, which could to overestimations of 28.9% at suburban sites in



1 spring (Jung et al., 2017). CO was measured using infrared absorption (Zhang and Cao.,
2 2015), and there were 1454 stations in China during the campaign period.

3 For validation of NO₂ and HCHO vertical column density, data from the Pandora
4 spectrometer were used, which the model reproduced with emission inventories at the
5 Olympic Park site (37.5232°N, 127.126°E). The HCHO data from Pandora is corrected
6 because of internal off-gasing to avoid positive biases (Spinei et al., 2021). At the same
7 observation site, surface NO₂ was also measured by a KENTEK NO_x analyzer with
8 photolytic method, and surface O₃ was measured using the same instrument. Ground-
9 based HCHO was measured using Aerodyne QCL. We compared the observed diurnal
10 cycle of vertical column and surface concentrations of NO₂ and HCHO with the model
11 simulations utilizing EDV2, EDV3, and KOV5. We also used ground-based VOC data
12 from gas chromatography flame ionization detector (GC-FID) operated by the Seoul
13 Research Institute of Public Health and Environment (SIHE).

14

15 **2.3.3. Aircraft data**

16 The DC-8 research aircraft, operated by NASA, performed multiple flight
17 measurements with a variety of measuring instruments. We utilized 1 minute interval
18 merged data of O₃, NO₂, CO, HCHO, and VOC along the 20 flight paths (Figure 7).
19 The nearest WRF-Chem grid is selected and then temporally and vertically interpolated
20 to the aircraft data to fully utilize the observations. Atmospheric NO₂ and O₃
21 concentrations were measured using a 4-channel chemiluminescence instrument, with
22 an uncertainty of 100 pptv + 30% and 5 ppbv + 10%, respectively. CO concentrations
23 were observed using a diode laser spectrometer, with an uncertainty of 2% or 2 ppbv.



1 The Compact Atmospheric Multi-species Spectrometer (CAMS) was used to measure
2 HCHO concentration, with a possible 3% systematic error (Richter et al., 2015). We
3 also utilized data from the Whole Air Sampler (WAS) to analyze VOC species from
4 different emission inventories (Colman et al., 2001). In this study, we focused on DC-
5 8 observations below a height of 2 km to concentrate on planetary boundary layer (PBL)
6 chemistry. The observation height was determined by GPS altitude above ground level.

7

8 **3. Results**

9 **3.1. The model meteorology simulations**

10 The model temperature and relative humidity were compared with surface observations
11 in China and South Korea. The model-simulated temperature had a slight negative mean
12 bias of -0.91 °C (correlation coefficient $R = 0.90$) in China, with the largest negative
13 bias in southwestern China. In South Korea, the mean bias was -1.71 °C ($R = 0.88$). The
14 simulated relative humidity showed a negative bias of -20 to -10% in the North China
15 Plain (NCP) area and a positive bias of 10 to 20% in southwestern China. There was a
16 negative bias of relative humidity over the west coastal area and a positive bias of 10 to
17 20% at most observation stations in South Korea. The correlation coefficients between
18 the model relative humidity and observations were 0.85 and 0.76 for China and South
19 Korea, respectively. Overall, the comparisons showed decent model simulations of
20 meteorology. During the KORUS-AQ campaign period, WRF-Chem accurately
21 simulated the daytime PBL height from a laser ceilometer (CL-31, Vaisla Inc., Finland)
22 observed at Yonsei University in Seoul, South Korea (Lee et al., 2019). But, Travis et
23 al. (2022) has indicated the possibility of PBL height underestimations by CTM.
24 Furthermore, due to limitations of the instrument, the ceilometer has potential to



1 inadequately estimate nighttime PBL height. It is primarily attributed to the method
2 based on aerosol gradients (Jordan et al., 2020). Therefore, the interpretation of
3 simulated nighttime concentrations of air pollutants should be approached with caution.
4 More analysis of meteorological fields, including PBL height, can be found in the
5 Supporting Information (Table S5 and Figure S2-S3).

6

7 **3.2. Evaluations with routine surface chemical observational data**

8 The study compared simulated concentrations of O₃, NO₂, and CO with data from
9 routine surface observational networks (Table 2 and Figure 2-6). First, the diurnal
10 variations of the model O₃ using different emissions inventories were compared with
11 observations for each subregion (Table 2 and Figure 2). Overall, all emissions
12 successfully reproduced diurnal variations and absolute values of O₃ for most regions,
13 but there were notable discrepancies in several regions. In the North China Plain (NCP)
14 region, EDV2 led to a negative model O₃ bias (-12 ppb) with R=0.65, while EDV3 and
15 KOV5 simulated O₃ better with reduced biases and increased correlations (R=0.68-
16 0.71). Similarly, EDV2 had a negative O₃ bias (-17 ppb) with R=0.62 in the Yangtze
17 River Delta (YRD) area, but EDV3 and KOV5 much improved the simulations, which
18 was also observed in the Northeastern China (NEC) area. However, the model O₃
19 concentrations based on the three emission inventories were overestimated in the
20 Sichuan-Chongqing-Guizhou (SCG) and Southeastern China (SEC) area. In Pearl River
21 Delta (PRD), EDV2 showed the lowest bias (-0.3 ppb) compared to EDV3 and KOV5.
22 In the suburban area of Northern China (NOC), all emission inventories reasonably
23 simulated hourly O₃ concentrations. Averaged O₃ was well simulated in South Korea
24 (KOR) with low biases (-1 to 0.7 ppb), but a negative bias appears over the Seoul



1 metropolitan area (SMA) with all emissions (-5.5 to -3.5 ppb) (Table 2).

2 The study also analyzed the mean values of daily maximum 8-hour average (MDA8)

3 O₃ concentration at each site and their spatial distributions for the entire campaign

4 period (Figure 3). The spatial distributions of the model MDA8 O₃ were not well

5 correlated with those of the observations. But, notable disparities were observed in

6 simulating MDA8 O₃ when the different emissions were used. For the north and eastern

7 part of China including Beijing and Shanghai, large negative biases disappear when

8 using EDV3 and KOV5. KOV5 only shows a significant correlation with the surface

9 MDA8 O₃ observations (including 929 sites) than EDV2 and EDV3 in China (0.43

10 versus 0.01, 0.20). The correlations between the time series of the model MDA8 O₃ and

11 observations varied at each site, with about 40-60% of sites (depending on the emission

12 inventories) showing a correlation coefficient greater than 0.6 (see Supporting

13 Information, Figure S4), and the locations of these sites were scattered. The correlation

14 slightly improved with hourly O₃ concentrations instead of MDA8 O₃, with about 50-

15 60% of sites having a correlation coefficient greater than 0.6 (Supporting Information,

16 Figure S4). For this metric, high correlations occurred in pollution hot spots north of

17 30°N and the South Coast of China, in which the ratio of HCHO to NO₂ (FNR) was

18 much less than 1, suggesting VOC-limited/NO_x-saturated chemical regime (Supporting

19 Information, Figure S5). The model MDA8 O₃ were underestimated for the pollution

20 hot spots with a low HCHO to NO₂ ratio located north of 30°N, suggesting a possibility

21 of model underestimations of anthropogenic VOC emissions causing model MDA8 O₃

22 biases at these sites. In contrast, the simulated MDA8 O₃ was generally overestimated

23 for sites south of 30°N in which HCHO concentrations were high (Supporting

24 Information, Figure S5). Zhang et al. (2020) reported that simulated biogenic isoprene



1 from MEGAN was overestimated compared to observation sites under 35°N in China.

2 The EDV2 and EDV3 showed a positive NO₂ bias over the YRD, NCP, and PRD
3 regions, which include large cities in China (Table 2 and Figure 4-5). On the other hand,
4 EDV2 and EDV3 had low negative NO₂ biases in the NEC and NOC regions (Figure
5 4). All models demonstrated reasonable NO₂ model performance in the SCG region,
6 where MDA8 O₃ was overestimated (Figure 2 and 4). In the YRD region, there were
7 large positive NO₂ biases with EDV2, EDV3, and KOV5 (ranging from 6.4 to 22.7 ppb).
8 Liu et al. (2021) reported that YRD is in a VOC-limited regime when using EDV2. The
9 findings indicated that a reduction in NO_x emissions led to an increase in O₃
10 concentrations, while a reduction in VOC emissions resulted in lower O₃
11 concentrations. The lower bias of O₃ in YRD can be attributed to the combined
12 influence of higher anthropogenic NO_x emissions and VOC originated from both
13 anthropogenic and biogenic sources (Figure S5). In contrast, KOV5 underestimated
14 NO₂ in the NCP region, while EDV2 and EDV3 did not. All emissions showed
15 significant discrepancies compared to NO₂ observations in the SEC area, with a low
16 correlation coefficient (0.19 to 0.26). EDV3 showed the lowest bias of -1.9 ppb (-0.8
17 ppb) compared to EDV2 and KOV5 in South Korea (SMA). The daily averaged NO₂
18 exhibited spatial distributions similar to MDA8 O₃ and CO (Figure 5). The slopes of
19 regression between the three model simulations and observations were 1.31, 1.03, and
20 0.8 for EDV2, EDV3, and KOV5, respectively, in China. The correlation coefficients
21 between the simulated NO₂ utilizing EDV2, EDV3, and KOV5 and surface data were
22 around 0.6 in China. EDV2, EDV3, and KOV5 demonstrated good correlations with
23 observations in South Korea (R = 0.69-0.74). Correlation coefficient (R) was the
24 highest with KOV5 in South Korea (R=0.74).



1 The simulated CO was averaged at each site and compared with observations
2 during the KORUS-AQ campaign period (Figure 6). The three model results showed
3 similar spatial distributions to observations, indicating higher CO concentrations in the
4 NCP, YRD, and PRD regions than their surrounding areas. However, all simulations
5 failed to reproduce the abundance of CO, indicating large negative biases throughout
6 the country. The bias was larger in South Korea than in China.

7

8 **3.3. Evaluations with the airborne and special surface chemical observations** 9 **during KORUS-AQ**

10

11 **3.3.1. The aircraft observations**

12 Figure 7 shows the flight paths flown by the DC-8 during the KORUS-AQ campaign
13 period. In Table 3, we compare the model results for O₃, NO₂, CO, HCHO, TOL, XYL,
14 ETE (Ethene or OL2), and ISO with the corresponding observed values for all flight
15 tracks under 2 km height in South Korea (Table 3). On average, the model
16 underestimated O₃ by 15-18 ppb, with EDV3 exhibiting the lowest O₃ bias (-15.1 ppb)
17 compared to EDV2 and KOV5 (-16.8 and -17.5 ppb, respectively). All emissions
18 showed positive biases for NO₂ (0.64 to 1.72 ppb), ETE (0.08 to 0.14 ppb), and ISO
19 (0.1 to 0.11 ppb). However, the model significantly underestimated CO, HCHO, TOL,
20 and XYL for all three emissions. Given the large spatial variability of air pollutants in
21 South Korea, we also sampled aircraft data from six regions (see Figure 7) and
22 compared the three model results with the aircraft observations under 2 km height
23 (Figure 8).

24 The flight tracks that surveyed large power plants and factories in the Chungnam
25 region on a daily basis are shown in Figure S6 in the Supporting Information. The



1 largest negative model O₃ bias was observed over the Chungnam region, with a
2 difference of 38-41 ppb. Emission estimation uncertainties can be significant over this
3 region, where there are large point sources such as coal-burning power plants and
4 petrochemical industries. The model NO₂ agreed with the aircraft observations in SMA,
5 but it tends to overestimate the measurements in the other areas. There were substantial
6 model overestimations of NO₂ with EDV3 over the Chungnam and Busan areas, while
7 KOV5 showed the most reasonable model NO₂ simulations. The model CO near the
8 surface was underestimated in the entire domain, resulting in high negative model CO
9 biases relative to the aircraft observations across the six regions (Figure 8). Additionally,
10 the model HCHO was underestimated by all emission inventories for all subregions,
11 with negative biases being evident in the SMA, Yellow Sea, and Chungnam regions.
12 Other model VOC species, such as TOL, XYL, ETE, and ISO, were also analyzed.
13 These VOC species are classified by their chemical structures and reactivities in the
14 RACM (Stockwell et al., 1997) (Table S2). For example, TOL includes toluene and
15 relatively less reactive aromatics, while XYL includes xylene and more reactive
16 aromatics. The WAS data from DC-8 were lumped into RACM (Supporting
17 Information Table S6, Lu et al., 2013) and were compared with aircraft observations.
18 When the model TOL or XYL was compared with the observed toluene and xylene, the
19 model using KOV5 reasonably reproduced the observed concentrations (light gray bars
20 in Figure 8). However, the model TOL (even using KOV5) underestimated the observed
21 lumped TOL for most of the regions except for Busan (bars including the dark gray part
22 in Figure 8). The model using KOV5 reasonably reproduced the observed xylene or
23 XYL, except for the Chungnam and Busan regions. The observed ethene (or ETE)
24 concentrations were low (< 0.5 ppb), except for the Chungnam region, where the



1 average of measurements was 2.1 ppb. The model ethene concentration was higher than
2 the observations for the SMA, Kyungbuk, and Busan regions, while it had a large
3 negative bias (-1.6 ~ -1.3 ppb) for the Chungnam region. Regarding isoprene (ISO), one
4 of the most important biogenic VOCs, the model values were larger than the
5 observations by a factor of 2. In summary, underestimated CO and aromatic VOCs are
6 the main features, along with underestimated ozone and HCHO. The largest
7 discrepancies occur over the Chungnam region, where large point sources are located
8 on the west coast of South Korea. The detailed statistics over the SMA and Chungnam
9 area can be obtained from the Supporting Information (Table S7-S8).

10 Figure 9 displays the vertical distributions of observed and simulated O₃ and related
11 species over SMA. The shapes of the simulated profile were in agreement with the
12 observations. Particularly, the model accurately reproduced the observed NO₂ profiles
13 though the surface NO₂ is underestimated by -4.2 to -0.8 ppb in SMA (Table 2 and
14 Figure 9b). The underestimation of simulated surface NO₂ is explained by the
15 overestimation of molybdenum converter method; surface concentrations of NO₂ from
16 molybdenum converter is larger than photolytic converter by 13.6% on average and 64%
17 at 4 pm (Figure 10). However, the simulated O₃ and HCHO had negative biases of 16.4
18 ppb and 0.73 ppb, respectively, persisting from the surface to 2 km. Additionally, the
19 simulated CO underestimated the observations by 40% throughout the vertical layer.
20 While the model TOL and XYL, utilizing KOV5, agreed well with the observations
21 below 1 km, the results using EDV2 and EDV3 substantially underestimated the
22 observations throughout the layer. On the other hand, the model simulated ETE and
23 ISO overestimated the observations below 1 km over SMA.

24



1 **3.3.2. The ground-based observations**

2 During the KORUS-AQ campaign, Pandora and surface measurements were co-located
3 at the Olympic Park. Figure 10 compares the observed diurnal cycle of Pandora vertical
4 columns and surface concentrations of NO₂ and HCHO with the model simulations.
5 The photolytic converter was used to measure surface NO₂ to minimize positive bias
6 from the molybdenum converter. All emissions reasonably simulated the diurnal
7 patterns of vertical column and surface NO₂ and HCHO concentrations. The surface
8 NO₂ peak appeared at 07 LT in the model and 08 LT in the observations, associated
9 with the increase of traffic and the under-developed convective boundary layer. On the
10 other hand, the Pandora NO₂ column amount increased from 06 LT to 12 LT and stayed
11 at that value throughout the afternoon, indicating the increase of NO_x emissions from
12 morning to afternoon. The model-simulated NO₂ columns agreed with those from
13 Pandora in terms of absolute values and diurnal variations. The opposite patterns
14 between surface and column NO₂ were also shown in Crawford et al. (2020). The
15 simulated and observed HCHO show similar diurnal variations, but all three emissions
16 underestimated both column and surface HCHO values by up to -8.5×10^{15}
17 molecules·cm⁻² (-46%) at 7 LT and -0.9 ppbv (-26%) at the surface on average. The
18 underestimations of the model HCHO relative to the Pandora and surface observations
19 are similar to findings from comparisons of the model results with the aircraft data
20 (Figure 9). Therefore, the model VOC performance needs to be investigated at the
21 Olympic Park.

22 The diurnal variations of the model O₃, CO, TOL, and XYL were evaluated against
23 the surface observations at the Olympic Park acquired during the KORUS-AQ
24 campaign (Figure 11). The diurnal pattern and hourly averaged mixing ratio of O₃ were



1 well simulated with the three emission inventories with slight model negative biases.
2 The observed CO was 2.7 times higher than the model on average. Considering the
3 diurnal profile of observed TOL and XYL, KOV5 reduced the model negative biases
4 from EDV2 and EDV3, but it still showed negative biases. The model TOL and XYL
5 showed peak concentrations at 08 LT, but the observation had a maximum value at 06
6 LT. The model biases of XYL (-3.7 to -0.6 ppb, -89 to -20%) were much larger than
7 those in TOL at the surface. Our study demonstrates that the improvement of VOC
8 emission/chemistry representations in the model is necessary for better simulations of
9 air quality over SMA and South Korea.

10

11 **3.4. The model performances for the Local and Transport Cases**

12 Previous studies have used meteorological conditions to classify synoptic patterns that
13 affect air pollutant concentrations (Park et al. 2021; Peterson et al. 2019). In contrast,
14 we defined the Transport and Local cases by comparing model results that used the
15 EDV3 base emission and the EDV3 zero-out-Chinese emission (see Figure 12). The
16 Local case comprises May 4, May 20, June 2, and June 3 (Supporting Information,
17 Figure S7), while the Transport case includes May 25, May 26, and May 31 (Supporting
18 Information, Figure S8). The Local (Transport) case in this study generally aligns with
19 the Stagnant and Blocking (Transport) cases in Peterson et al. (2019). The Local case
20 has a Chinese contribution to O₃ of under 11%, whereas the Transport case has a
21 Chinese contribution to O₃ of over 46%. EDV3 performed better in simulating O₃ for
22 the Transport case compared to EDV2 and KOV5, with a bias of only 2.7 ppb in
23 comparison with the DC-8 airborne observations. In contrast, for the Local case, all
24 emissions had a negative bias ranging from 15.5-18.2 ppb. See the Table S9 in



1 Supporting Information to obtain detailed information of model performances against
2 DC-8 measurements for different cases. Surface concentrations of O₃ at Olympic Park
3 also exhibited enhanced contributions from Chinese anthropogenic emissions for
4 Transport case (Figure S9). This section focuses on the model simulations using EDV3
5 and its modified versions, EDV3_Ch2 and EDV3_ChKo2 (doubling Chinese and South
6 Korean CO and VOC emissions).

7 Figure 13 illustrates the biases in the model O₃, CO, and HCHO using EDV3 and
8 its variants relative to DC-8 observations over SMA. The plot highlights differences in
9 biases for the Local and Transport cases. The model O₃ biases were negative, and the
10 absolute values of biases were larger in the Local case than in the Transport case (-20%
11 versus -6%). The model CO biases were also negative, and the absolute values of biases
12 were larger in the Transport case than in the Local case. The model HCHO biases were
13 negative and similar for the two cases, except for a larger discrepancy between model
14 and observation in the Local case than in the Transport case. Doubling Chinese CO and
15 VOC emissions (EDV3_Ch2) only slightly reduced biases in the Local case, whereas
16 doubling South Korean CO and VOC emissions, as well as Chinese CO and VOC
17 emissions (EDV3_ChKo2), were necessary to substantially reduce the model biases for
18 the Local case. For the Transport case, doubling Chinese CO and VOC emissions
19 reduced biases to almost zero for CO and HCHO, but the model O₃ was much
20 overestimated, with 14% positive biases (from an original bias of -6%). Further
21 increasing South Korean CO and VOC emissions led to overestimations of O₃ (20%)
22 and HCHO (33%). These sensitivity tests modifying EDV3 indicate that increases in
23 CO and VOC emissions over South Korea improve the model O₃, CO, and VOC
24 simulations. However, increasing Chinese VOC (and CO) emissions may overestimate



1 the model O₃ for the studied period.

2

3 **4. Summary and conclusions**

4 We conducted sensitivity tests using WRF-Chem with three different bottom-up
5 emission inventories (EDGAR-HTAP v2, v3, and KORUS v5) to investigate the
6 impacts of different emissions on the simulation of O₃ and precursors in East Asia. This
7 study is the first to use EDGAR-HTAP v3 with WRF-Chem v4.4 and extends the
8 validation domain to the whole of China during the KORUS-AQ campaign period. We
9 extensively validated these emission inventories using both ground and aircraft
10 observations in East Asia.

11 The three emission inventories accurately reproduced the diurnal profiles and
12 absolute values of surface O₃ for most subregions in China, except for the SCG and
13 SEC areas. However, discrepancies were observed in the model performance for the
14 MDA8 O₃ concentrations, with poor correlations observed over regions with high
15 HCHO concentrations (south of 30°N) and relatively low ratios of FNR (north of 30°N).
16 The emission inventories reasonably reproduced the spatial distribution of daily surface
17 NO₂ concentrations. However, we found that CO was considerably underestimated by
18 the emission inventories over both China and South Korea.

19 We evaluated the model simulations against vertical profile measurements of O₃,
20 NO₂, CO, HCHO, TOL, XYL, ETE, and ISO from the DC-8 aircraft, as well as surface
21 observations over South Korea. The simulated vertical shapes of O₃, NO₂, CO, HCHO,
22 TOL, XYL, ETE, and ISO agreed well with the DC-8 measurements in the SMA,
23 although negative biases were observed for O₃, CO, TOL, XYL, and HCHO, with the



1 largest discrepancy between the model results and observations in the Chungnam area.
2 When we compared the simulations with the surface in-situ measurements and
3 PANDORA observations at the Olympic Park in Seoul, the model accurately
4 reproduced the diurnal patterns of surface and vertical columns of NO₂ and HCHO.
5 However, we found that the model underestimated TOL and XYL. This underestimation
6 of TOL and XYL is one of the reasons why the model underestimates O₃ concentrations,
7 as VOCs contribute to NO to NO₂ conversions resulting in O₃ production via
8 photochemistry.

9 We also classified the flight tracks into two categories: Local and Transport cases.
10 We found that the negative bias of O₃ was much larger under the Local case than the
11 Transport case. When the increment of CO and VOC emissions in South Korea is taken
12 into account, the biases of O₃ are significantly reduced, indicating the need for local
13 emission adjustments to decrease O₃ bias in South Korea.

14 Our study revealed a consistent overestimation of isoprene over SMA. The
15 uncertainty of biogenic VOC emissions from MEGAN can affect the model O₃
16 performance. Therefore, to achieve more accurate simulations of O₃ in East Asia, it is
17 essential to explore precise representations of both anthropogenic and biogenic VOC
18 emissions.

19

20 **Code and data availability**

21 WRF-Chem source codes are distributed by NCAR (<https://doi:10.5065/D6MK6B4K>).
22 WRF-Chem v4.4 is available in the GitHub (wrf-model, 2022). The exact version of
23 WRF-Chem codes and configuration files are archived at



1 <https://doi.org/10.5281/zenodo.8260026> (Kim et al., 2023). National Centers for
2 Environmental Prediction (NCEP) FNL data can be accessed from Research Data
3 Archive (RDA) (NCEP, 2019). The CAM-Chem data for boundary conditions is also
4 obtained from RDA (ACOM, 2019). The EDGAR-HTAP v2 data can be downloaded
5 in the website (https://edgar.jrc.ec.europa.eu/dataset_htap_v2). The EDGAR-HTAP v3
6 is archived on Zenodo (Crippa, 2023). The KORUS-AQ data are available in the
7 website (<https://www-air.larc.nasa.gov/cgi-bin/ArcView/korusaq>)
8 (doi:10.5067/Suborbital/KORUSAQ/DATA01). The EDGAR-HTAP v2, v3, and
9 KORUS v5 data including emission processing programs are available at
10 <https://doi.org/10.5281/zenodo.8260026> (Kim et al., 2023).

11

12 **Author contribution**

13 KMK conducted simulations, analysis and wrote the paper. SWK designed this study,
14 secured funding, performed analysis and wrote the paper. SS supported model set-up
15 and contributed to refining the paper. DRB measured VOC data from DC-8. SC
16 acquired ground-based in-situ VOC data at Olympic Park. JHC performed analysis and
17 wrote the paper. LE and GF assisted in setting up the model emissions and discussed
18 about the model performance. AF measured HCHO data from DC-8. JRH measured
19 Pandora data (NO₂, HCHO). JH retrieved PBL height and discussed about the results.
20 JJ acquired NO₂ data at Olympic Park with different methods. AJW acquired NO₂ and
21 O₃ data from DC-8. JHW and QZ provided emissions inventories and related
22 information. All authors reviewed the manuscript.

23



1 **Competing interests**

2 At least one of the (co-)authors is a member of the editorial board of Geoscientific
3 Model Development.

4

5 **Acknowledgements**

6 This work was supported by the National Research Foundation of Korea (NRF) grant
7 funded by the Korea government (MSIT) (No. 2020R1A2C2014131). S.-W. Kim also
8 acknowledges support from NRF-2018R1A5A1024958. All the computing resources
9 are provided by National Center for Meteorological Supercomputer. The National
10 Center for Atmospheric Research (NCAR) is sponsored by the National Science
11 Foundation (NSF) (NNX16AD96G). We would like to express our gratitude to Glen
12 Diskin for generously providing the CO data from the DC-8 aircraft. We also thanks to
13 Andrew Whitehill and Russell Long for providing the HCHO data from Olympic Park.
14 We would also like to thank Meng Li and Brian McDonald for their valuable
15 discussions, which greatly enhanced our understandings.

16

17 **References**

- 18 Ackermann, I. J., Hass, H., Memmesheimer, M., Ebel, A., Binkowski, F. S., and
19 Shankar, U.: Modal aerosol dynamics model for Europe: Development and first
20 applications, *Atmos. Environ.*, 32, 2981-2999, [https://doi.org/10.1016/S1352-](https://doi.org/10.1016/S1352-2310(98)00006-5)
21 [2310\(98\)00006-5](https://doi.org/10.1016/S1352-2310(98)00006-5), 1998.
- 22 Ahmadov, R., McKeen, S. A., Robinson, A. L., Bahreini, R., Middlebrook, A. M., de
23 Gouw, J. A., Meagher, J., Hsie, E.-Y., Edgerton, E., Shaw, S., and Trainer, M.: A
24 volatility basis set model for summertime secondary organic aerosols over the eastern
25 United States in 2006, *J. Geophys. Res. Atmos.*, 117, D06301,
26 <https://doi.org/10.1029/2011JD016831>, 2012.
- 27 Anenberg, S. C., Henze, D. K., Tinney, V., Kinney, P. L., Raich, W., Fann, N., Malley,
28 C. S., Roman, H., Lamsal, L., Duncan, B., Martin, R. V., van Donkelaar, A., Brauer,
29 M., Doherty, R., Jonson, J. E., Davila, Y., Sudo, K., and Kuylentierna, J. C.I.:
30 Estimates of the global burden of ambient PM_{2.5}, Ozone, and NO₂ on asthma
31 incidence and emergency room visits, *Environ. Health Perspect.*, 126, 107004,
32 doi.org/10.1289/EHP3766, 2018.



- 1 Atmospheric Chemistry Observations & Modeling/National Center for Atmospheric
2 Research/University Corporation for Atmospheric Research. 2020. CESM2.1 The
3 Community Atmosphere Model with Chemistry (CAM-chem) Outputs as Boundary
4 Conditions. Research Data Archive at the National Center for Atmospheric Research,
5 Computational and Information Systems Laboratory. [https://doi.org/10.5065/CKR4-](https://doi.org/10.5065/CKR4-GP38)
6 [GP38](https://doi.org/10.5065/CKR4-GP38). Accessed: 16 April 2019.
- 7 Buchholz, R. R., Emmons, L. K., Tilmes, S., and The CESM2 Development Team,
8 (2019). CESM2.1/CAM-chem Instantaneous Output for Boundary Conditions.
9 UCAR/NCAR - Atmospheric Chemistry Observations and Modeling Laboratory. Lat:
10 -5 to 45, Lon: 75 to 145, 28 Nov 2022, doi.org/10.5065/NMP7-EP60.
- 11 Carter, W. P.: Documentation of the SAPRC-99 chemical mechanism for VOC
12 reactivity assessment, Contract, 92, 95–308,
13 <https://intra.engr.ucr.edu/~carter/pubs/s99doc.pdf> (last access: 9 June 2023), 2000.
- 14 Chen, S.-H. and Sun, W.-Y.: A one-dimensional time dependent cloud model, *J.*
15 *Meteorol. Soc. Japan*, 80, 99-118, <https://doi.org/10.2151/jmsj.80.99>, 2002.
- 16 Colman, J. J., Swanson, A. L., Meinardi, S., Sive, B. C., Blake, D. R., and Rowland, F.
17 S.: Description of the analysis of a wide range of volatile organic compounds in
18 Whole Air Samples collected during PEM-Tropics A and B, *Anal. Chem.*, 73, 3723-
19 3731, <https://doi.org/10.1021/ac010027g>, 2001.
- 20 Crawford, J. H., Ahn, J.-Y., Al-Saadi, J., Chang, L., Emmons, L. K., Kim, J., Lee, G.,
21 Park, J.-H., Park, R. J., Woo, J. H., Song, C.-K., Hong, J.-H., Hong, Y.-D., Lefer, B.
22 L., Lee, M., Lee, T., Kim, S., Min, K.-E., Yum, S. S., Shin, H. J., Kim, Y.-W., Choi,
23 J.-S., Park, J.S., Szykman, J. J., Long, R. W., Jordan, C. E., Simpson, I. J., Fried, A.,
24 Dibb, J. E., Cho, S., and Kim, Y. P.: The Korea-United States Air Quality (KORUS-
25 AQ) field study, *Elem. Sci. Anth.*, 9, 00163,
26 <https://doi.org/10.1525/elementa.2020.00163>, 2020.
- 27 Crippa, M., Guizzardi, D., Butler, T., Keating, T., Wu, R., Kaminski, J., Kuenen, J.,
28 Kurokawa, J., Chatani, S., Morikawa, T., Pouliot, G., Racine, J., Moran, M. D.,
29 Klimont, Z., Manseau, P. M., Mashayekhi, R., Henderson, B. H., Smith, S. J.,
30 Suchyta, H., Muntean, M., Solazzo, E., Banja, M., Schaaf, E., Pagani, F., Woo, J.-H.,
31 Kim, J., Monforti-Ferrario, F., Pisoni, E., Zhang, J., Niemi, D., Sassi, M., Ansari, T.,
32 and Foley, K.: The HTAP_v3 emission mosaic: merging regional and global monthly



- 1 emissions (2000–2018) to support air quality modelling and policies, *Earth Syst. Sci.*
2 *Data*, 15, 2667–2694, <https://doi.org/10.5194/essd-15-2667-2023>, 2023.
- 3 Crippa Monica. (2023). HTAP_v3 emission mosaic [edgar_HTAPv3_2016_*]. Zenodo.
4 <https://doi.org/10.5281/zenodo.7516361>
- 5 Dunlea, E. J., Herndon, S. C., Nelson, D. D., Volkamer, R. M., San Martini, F., Sheehy,
6 P. M., Zahniser, M. S., Shorter, J. H., Wormhoudt, J. C., Lamb, B. K., Allwine, E. J.,
7 Gaffney, J. S., Marley, N. A., Grutter, M., Marquez, C., Blanco, S., Cardenas, B.,
8 Retama, A., Ramos Villegas, C. R., Kolb, C. E., Molina, L. T., and Molina, M. J.:
9 Evaluation of nitrogen dioxide chemiluminescence monitors in a polluted urban
10 environment, *Atmos. Chem. Phys.*, 7, 2691–2704, [https://doi.org/10.5194/acp-7-](https://doi.org/10.5194/acp-7-2691-2007)
11 [2691-2007](https://doi.org/10.5194/acp-7-2691-2007), 2007.
- 12 Emmons, L. K., Walters, S., Hess, P. G., Lamarque, J.-F., Pfister, G. G., Fillmore, D.,
13 Granier, C., Guenther, A., Kinnison, D., Laepple, T., Orlando, J., Tie, X., Tyndall, G.,
14 Wiedinmyer, C., Baughcum, S. L., and Kloster, S.: Description and evaluation of the
15 Model for Ozone and Related chemical Tracers, version4(MOZART-4), *Geosci.*
16 *Model Dev.*, 3, 43–67, <https://doi.org/10.5194/gmd-3-43-2010>, 2010.
- 17 Emmons, L. K., Schwantes, R. H., Orlando, J. J., Tyndall, G., Kinnison, D., Lamarque,
18 J.-F., Marsh, D., Mills, M. J., Tilmes, S., Bardeen, C., Buchholz, R. R., Conley, A.,
19 Gettelman, A., Garcia, R., Simpson, I., Blacke, D. R., Meinardi, S., and Pétron, G.:
20 The Chemistry Mechanism in the Community Earth System Model version 2
21 (CESM2), *J. Adv. Model. Earth Syst.*, 12, e2019MS001882,
22 <https://doi.org/10.1029/2019MS001882>, 2020.
- 23 Franklin, B. A., Brook, R., and Arden Pope III, C.: Air Pollution and Cardiovascular
24 Disease, *Curr. Probl. Cardiol.*, 40, 207–238,
25 <https://doi.org/10.1016/j.cpcardiol.2015.01.003>, 2015.
- 26 Gaubert, B., Emmons, L. K., Raeder, K., Tilmes, S., Miyazaki, K., Arellano Jr., A. F.,
27 Elguindi, N., Granier, C., Tang, W., Barré, J., Worden, H. M., Buchholz, R. R.,
28 Edwards, D. P. Franke, P., Anderson, J. L., Saunois, M., Schroeder, J., Woo, J.-H.,
29 Simpson, I. J., Blake, D. R., Meinardi, S., Wennberg, P. O., Crounse, J., Teng, A.,
30 Kim, M., Dickerson, R. R., He, H., Ren X., Pusede, S. E., and Diskin, G. S.:
31 Correcting model biases of CO in East Asia: impact on oxidant distributions during



- 1 KORUS-AQ, *Atmos. Chem. Phys.*, 20, 14617–14647, [https://doi.org/10.5194/acp-](https://doi.org/10.5194/acp-20-14617-2020)
2 20-14617-2020, 2020.
- 3 Grell, G. A.: Prognostic evaluation of assumptions used by cumulus parameterizations,
4 *Mon. Weather Rev.*, 121, 764–787, [https://doi.org/10.1175/1520-](https://doi.org/10.1175/1520-0493(1993)121<0764:PEOAUB>2.0.CO;2)
5 0493(1993)121<0764:PEOAUB>2.0.CO;2, 1993.
- 6 Grell, G. A. and Dévényi, D.: A generalized approach to parameterizing convection
7 combining ensemble and data assimilation techniques, *Geophys. Res. Lett.*, 29, 38-
8 1-38-4, <https://doi.org/10.1029/2002GL015311>, 2002.
- 9 Grell, G. A., Peckham, S. E., Schmitz, R., McKeen, S. A., Frost, G., Shamarock, W. C.,
10 and Eder, B.: Fully coupled “online” chemistry within the WRF model, *Atmos.*
11 *Environ.*, 39, 6957–6975, <https://doi.org/10.1016/j.atmosenv.2005.04.027>, 2005.
- 12 Guenther, A., Karl, T., Harley, P., Wiedinmyer, C., Palmer, P. I., and Geron, C.:
13 Estimates of global terrestrial isoprene emissions using MEGAN (Model of
14 Emissions of Gases and Aerosols from Nature), *Atmos. Chem. Phys.*, 6, 3181–3210,
15 <https://doi.org/10.5194/acp-6-3181-2006>, 2006.
- 16 Hong, S.-Y. and Noh, Y.: A new vertical diffusion package with an explicit treatment of
17 entrainment processes, *Mon. Weather Rev.*, 134, 2318–2341,
18 <https://doi.org/10.1175/MWR3199.1>. 2006.
- 19 Jang, Y., Lee, Y., Kim, J., Kim, Y., and Woo, J.-H.: Improvement China point source for
20 improving bottom-up emission inventory, *Asia-Pac. J. Atmos. Sci.*, 56, 107–118,
21 <https://doi.org/10.1007/s13143-019-00115-y>, 2020.
- 22 Janssens-Maenhout, G., Crippa, M., Guizzardi, D., Dentener, F., Muntean, M., Pouliot,
23 G., Keating, T., Zhang, Q., Kurokawa, J., Wankmüller, R., van der Gon, H. D.,
24 Kuenen J. J. P., Kilmont, Z., Frost, G., Darras, S., Koffi, B., and Li, M.: HTAP_v2.2:
25 a mosaic of regional and global emission grid maps for 2008 and 2010 to study
26 hemispheric transport of air pollution, *Atmos. Chem. Phys.*, 15, 11411–11432,
27 <https://doi.org/10.5194/acp-15-11411-2015>, 2015.
- 28 Jordan, C. E., Crawford, J. H., Beyersdorf, A. J., Eck, T. F., Halliday, H. S., Vault, B.
29 A., Chang, L.-S., Park, J., Park, R., Lee, G., Kim, H., Ahn, J.-Y., Cho, S., Shin, H. J.,
30 Lee, J. H., Jung, J., Kim, D.-S., Lee, M., Lee, T., Whitehill, A., Szykman, J.,
31 Schueneman, M K., Campuzano-Jost, P., Jimenez, J. L., DiGangi, J. P., Diskin, G. S.,
32 Anderson, B. E., Moore, R. H., Ziemba, L. D., Fenn, M. A., Hair, J. W., Kuehan, R.



- 1 E., Holz, R. E., Chen, G., Travis, K., Shook, M., Peterson, D. A., Lamb, K. D., and
2 Schwarz, J. P.: Investigation of factors controlling PM_{2.5} variability across the South
3 Korean Peninsula during KORUS-AQ, *Elem. Sci. Anth.*, 8,
4 <https://doi.org/10.1525/elementa.424>, 2020.
- 5 Jung, J., Lee, J., Kim, B., and Oh, S.: Seasonal variations in the NO₂ artifact from
6 chemiluminescence measurements with a molybdenum converter at a suburban site
7 in Korea (downwind of the Asian continental outflow) during 2015-2016, *Atmos.*
8 *Environ.*, 165, 290-300, <https://doi.org/10.1016/j.atmosenv.2017.07.010>, 2017.
- 9 Kim, K.-M., Kim, S.-W., Choi, M., Kim, M., Kim J., Shina, I., Kim, J., Chung, C.Y.,
10 Yeo, H., Kim, S.-W., Joo, S. J., MckKeen, S. A., and Zhang, L.: Modeling Asian Dust
11 Storms Using WRF-Chem During the DRAGON-Asia Field Campaign in April 2012,
12 *J. Geophys. Res. Atmos.*, 126, e2021JD034793,
13 <https://doi.org/10.1029/2021JD034793>, 2021.
- 14 Kim, K.-M., Kim, S.-W., Seo, S., Blake, D. R., Cho, S., Crawford, J. H., Emmons, L.,
15 Fried, A., Herman, J. H., Hong, J., Jung, J., Pfister, G., Weinheimer, A. J., Woo, J.-
16 H., and Zhang, Q.: WRF-Chem configurations and input data sets for sensitivity tests
17 of emission inventories, Zenodo [Data set], <https://doi.org/10.5281/zenodo.8260026>,
18 2023.
- 19 Kim, S.-W., McDonald, B. C., Baidar, S., Brown, S. S., Dube, B., Ferrare, R. A., Frost,
20 G. J., Harley, R. A., Holloway, J. S., Lee, H.-J., McKeen, S. A., Neuman, J. A., Bowak,
21 J. B., Oetjen, H., Ortega, I., Pollack, I. B., Roberts, J. M., Ryerson, T. B., Scarino, A.
22 J., Senff, C. J., Thalman, R., Trainer, M., Volkamer, R., Wagner, N., Washenfelder, R.
23 A., Waxman, E., and Young, C. J.: Modeling the weekly cycle of NO_x and CO
24 emissions and their impacts on O₃ in the Los Angeles-South Coast Air Basin during
25 the CalNex 2010 field campaign, *J. Geophys. Res. Atmos.*, 121, 1340-1360,
26 <https://doi.org/10.1002/2015JD024292>, 2016.
- 27 Kwon, H.-A., Park, R. J., Oak, Y. J., Nowlan, C. R., Janz, S. J., Kowalewski, M. G.,
28 Fried, A., Walega, J., Bates, K. H., Choi, J., Blake, D. R., Wisthaler, A., and Woo, J.-
29 H.: Top-down estimates of anthropogenic VOC emissions in South Korea using
30 formaldehyde vertical column densities from aircraft during the KORUS-AQ
31 campaign, *Elem. Sci. Anth.*, 9, 00109, <https://doi.org/10.1525/elementa.2021.00109>,
32 2021.



- 1 Kurokawa, J. and Ohara, T.: Long-term historical trends in air pollutant emissions in
2 Asia: Regional Emission inventory in ASia (REAS) version 3, *Atmos. Chem. Phys.*,
3 20, 12761-12793, <https://doi.org/10.5194/acp-20-12761-2020>, 2020.
- 4 Lee, B.-J., Kim, B., and Lee, K.: Air pollution exposure and cardiovascular disease,
5 *Toxicol. Res.*, 30, 71-75, <https://doi.org/10.5487/TR.2014.30.2.071>, 2014.
- 6 Lee, J. H., Hong, J.-W., Lee, K. M., Hong, J., Velasco, E., Lim, Y., Lee, J., Nam, K.,
7 and Park, J.: Ceilometer monitoring of boundary layer height in Seoul and its
8 application to evaluate the dilution effect on air pollution, *Boundary Layer Meteorol.*,
9 171, 435-455, <https://doi.org/10.1007/s10546-019-00452-5>, 2019.
- 10 Li, M., Zhang, Q., Streets, D. G., He, K. B., Cheng, Y. F., Emmons, L. K., Huo, H.,
11 Kang, S. C., Lu, Z., Shao, M., Su, H., Yu, X., and Zhang, Y.: Mapping Asian
12 anthropogenic emissions of non-methane volatile organic compounds to multiple
13 chemical mechanisms, *Atmos. Chem. Phys.*, 14, 5617-5638,
14 <https://doi.org/10.5194/acp-14-5617-2014>, 2014.
- 15 Li, Q., Zhang, L., Wang, T., Tham, Y. J., Ahmadov, R., Xue, L., Zhang, Q., and Zheng,
16 J.: Impacts of heterogeneous uptake of dinitrogen pentoxide and chlorine activation
17 on ozone and reactive nitrogen partitioning: improvement and application of the
18 WRF-Chem model in southern China, *Atmos. Chem. Phys.*, 16, 14875-14890,
19 <https://doi.org/10.5194/acp-16-14875-2016>, 2016.
- 20 Liu, Z., Doherty, R. M., Wild, O., Hollaway, M., and O'Connor, F. M.: Contrasting
21 chemical environments in summertime for atmospheric ozone across major Chinese
22 industrial regions: the effectiveness of emission control strategies, *Atmos. Chem.*
23 *Phys.*, 21, 10689-10706, <https://doi.org/10.5194/acp-21-10689-2021>, 2021.
- 24 Lu, K. D., Hofzumahaus, A., Holland, F., Bohn, B., Brauers, T., Fuchs, H., Hu, M.,
25 Häseler, R., Kita, K., Kondo, Y., Li, X., Lou, S. R., Oebel, A., Shao, M., Zheng, J.
26 M., Wahner, A., Zhu, T., Zhang, T. H., and Rohrer, F.: Missing OH source in a
27 suburban environment near Beijing: observed and modelled OH and HO₂
28 concentrations in summer 2006, *Atmos. Chem. Phys.*, 13, 1057-1080,
29 doi.org/10.5194/acp-13-1057-2013, 2013.
- 30 Madronich, S.: Photodissociation in the Atmosphere, 1, actinic flux and the effects of
31 ground reflections and clouds, *J. Geophys. Res. Atmos.*, 92, 9740-9752.
32 <https://doi.org/10.1029/JD092iD08p09740>, 1987.



- 1 Manning, W. J. and von Tiedemann, A. Climate change: Potential effects of increased
2 atmospheric carbon dioxide (CO₂), ozone (O₃), and ultraviolet-B (UV-B) radiation
3 on plant diseases, *Environ. Pollut.*, 88, 219-245, <https://doi.org/10.1016/0269->
4 7491(95)91446-R, 1995.
- 5 National Centers for Environmental Prediction/National Weather Service/NOAA/U.S.
6 Department of Commerce. 2000, updated daily. NCEP FNL Operational Model
7 Global Tropospheric Analyses, continuing from July 1999. Research Data Archive at
8 the National Center for Atmospheric Research, Computational and Information
9 Systems Laboratory. <https://doi.org/10.5065/D6M043C6>. Accessed: 25 March 2019.
- 10 Park, R. J., Oak, Y. J., Emmons, L. K., Kim, C.-H., Pfister, G. G., Carmichael, G. R.,
11 Saide, P. E., Cho, S.-Y., Kim, S., Woo, J.-H., Crawford, J. H., Gaubert, B., Lee, H.-
12 J., Park, S.-Y., Jo, Y.-J., Gao, M., Tang, B., Stanier, C. O., Shin, S. S., Park, H. Y.,
13 Bae, C., and Kim, E.: Multi-model intercomparisons of air quality simulations for
14 the KORUS-AQ campaign, *Elem. Sci. Anth.*, 9, 00139,
15 <https://doi.org/10.1525/elementa.2021.00139>, 2021.
- 16 Peterson, D. A., Hyer, E. J., Han, S.-O., Crawford, J. H., Park, R. J., Holz, R., Kuehn,
17 R. E., Eloranta, E., Knute, C., Jordan, C. E., and Lefer, B. L.: Meteorology
18 influencing springtime air quality, pollution transport, and visibility in Korea, *Elem.*
19 *Sci. Anth.*, 7, 57, <https://doi.org/10.1525/elementa.395>, 2019.
- 20 Richter, D., Weibring, P., Walega, J. G., Fried, A., Supler, S. M., and Taubman, M. S.:
21 Compact highly sensitive multi-species airborne mid-IR spectrometer, *Appl. Phys. B*,
22 119, 119-131, <https://doi.org/10.1007/s00340-015-6038-8>, 2015.
- 23 Rosenzweig, C., Karoly, D., Vicarelli, M., Neofotis, P., Wu, Q., Casassa, G., Menzel,
24 A., Root, T. L., Estrella, N., Seguin, B., Tryjanowski, P., Liu, C., Rawlins, S., and
25 Imeson, A.: Attributing physical and biological impacts to anthropogenic climate
26 change, *Nature*, 453, 353-357, <https://doi.org/10.1038/nature06937>, 2008.
- 27 Saikawa, E., Kim, H., Zhong, M., Avramov, A., Zhao, Y., Janssens-Maenhout, G.,
28 Kurokawa, J.-I., Klimont, Z., Wagner, F., Naik, V., Horowitz, L. W., and Zhang, Q.:
29 Comparison of emissions inventories of anthropogenic air pollutants and greenhouse
30 gases in China, *Atmos. Chem. Phys.*, 17, 6393-6421, <https://doi.org/10.5194/acp-17->
31 6393-2017, 2017.



- 1 Sharma, A., Ojha, N., Pozzer, A., Mar, K. A., Beig, G., Lelieveld, J., and Gunthe, S. S.:
2 WRF-Chem simulated surface ozone over south Asia during the pre-monsoon:
3 effects of emission inventories and chemical mechanisms, *Atmos. Chem. Phys.*, 17,
4 14393-14414, <https://doi.org/10.5194/acp-17-14393-2017>, 2017.
- 5 Sicard, P., Crippa, P., De Marco, A., Castruccio, S., Giani, P., Cuesta, J., Paoletti, E.,
6 Feng, Z., and Anav, A.: High spatial resolution WRF-Chem model over Asia: Physics
7 and chemistry evaluation, *Atmos. Environ.*, 244, 118004,
8 <https://doi.org/10.1016/j.atmosenv.2020.118004>, 2021.
- 9 Spinei, E., Tiefengraber, M., Müller, M., Gebetsberger, M., Cede, A., Valin, L.,
10 Szykman, J., Whitehill, A., Kotsaki, A., Santos, F., Abbuhasan, N., Zhao, X., Fioletov,
11 V., Lee, S. C., and Swap, R.: Effect of polyoxymethylene (POM-H Delrin) off-
12 gassing within the Pandora head sensor on direct-sun and multi-axis formaldehyde
13 column measurements in 2016–2019, *Atmos. Meas. Tech.*, 14, 647-663,
14 <https://doi.org/10.5194/amt-14-647-2021>, 2021.
- 15 Stockwell, W. R., Kirchner, F., and Kuhn, M.: A new mechanism for regional
16 atmospheric chemistry modeling, *J. Geophys. Res. Atmos.*, 102, 25847-25879,
17 <https://doi.org/10.1029/97JD00849>, 1997.
- 18 Tewari, M., F. Chen, W. Wang, J. Dudhia, M. A. LeMone, K. Mitchell, M. Ek, G. Gayno,
19 J. Wegiel, and Cuenca, R. H.: Implementation and verification of the unified NOAA
20 land surface model in the WRF model, *20th conference on weather analysis and
21 forecasting/16th conference on numerical weather prediction*, pp. 11–15, 2004.
- 22 Travis, K. R., Crawford, J. H., Chen, G., Jordan, C. E., Nault, B. A., Kim, H., Jimenez,
23 J. L., Campuzano-Jost, P., Dibb, J. E., Woo, J.-H., Kim, Y., Zhai, S., Wang, X.,
24 McDuffie, E. E., Luo, G., Yu, F., Kim, S., Simpson, I. J., Blake, D. R., Chang, L.,
25 and Kim, M. J.: Limitations in representation of physical processes prevent
26 successful simulation of PM_{2.5} during KORUS-AQ, *Atmos. Chem. Phys.*, 22, 7933–
27 7958, <https://doi.org/10.5194/acp-22-7933-2022>, 2022.
- 28 Wada, A., Matsueda, H., Murayama, S., Taguchi, S., Kamada, A., Nosaka, M., Tsuboi,
29 K., and Sawa, Y.: Evaluation of anthropogenic emissions of carbon monoxide in East
30 Asia derived from the observations of atmospheric radon-222 over the western North
31 Pacific, *Atmos. Chem. Phys.*, 12, 12119–12132, <https://doi.org/10.5194/acp-12-12119-2012>, 2012.



- 1 Wild, O., Prather, M. J., and Akimoto, H.: Indirect long-term global radiative cooling
2 from NO_x Emissions, *Geophys. Res. Lett.*, 28, 1719-1722,
3 <https://doi.org/10.1029/2000GL012573>, 2001.
- 4 Woo, J.-H., Choi, K.-C., Kim, H. K., Baek, B. H., Jang, M., Eum, J.-H., Song, C. H.,
5 Ma, Y.-I., Sunwoo, Y., Chang, L.-S., and Yoo, S. H.: Development of an
6 anthropogenic emissions processing system for Asia using SMOKE, *Atmos. Environ.*,
7 58, 5-13, <https://doi.org/10.1016/j.atmosenv.2011.10.042>, 2012.
- 8 wrf-model: WRF, Github [code], <https://github.com/wrf-model/WRF/releases/tag/v4.4>,
9 last access: 18 May 2022.
- 10 Zhang, Y.-L. and Cao, F.: Fine particulate matter (PM_{2.5}) in China at a city level, *Sci.*
11 *Rep.*, 5, 14884, <https://doi.org/10.1038/srep14884>, 2015.
- 12 Zhang, Y., Zhang, R., Yu, J., Zhang, Z., Yang, W., Zhang, H., Lyu, S., Wang, Y., Dai,
13 W., Wang, Y., and Wang, X.: Isoprene Mixing Ratios Measured at Twenty Sites in
14 China During 2012–2014: Comparison With Model Simulation, *J. Geophys. Res.*
15 *Atmos.*, 125, e2020JD033523, <https://doi.org/10.1029/2020JD033523>, 2020.
- 16 Zheng, B., Tong, D., Li, M., Liu, F., Hong, C., Geng, G., Li, H., Li, X., Peng, L., Qi, J.,
17 Yan, L., Zhang, Y., Zhao, H., Zheng, Y., He, K., and Zhang, Q.: Trends in China's
18 anthropogenic emissions since 2010 as the consequence of clean air actions, *Atmos.*
19 *Chem. Phys.*, 18, 14095–14111, <https://doi.org/10.5194/acp-18-14095-2018>, 2018.
- 20 Zhong, M., Saikawa, E., Liu, Y., Naik, V., Horowitz, L. W., Takigawa, M., Zhao, Y.,
21 Lin, N.-H., and Stone, E. A.: Air quality modeling with WRF-Chem v3.5 in East Asia:
22 sensitivity to emissions and evaluation of simulated air quality, *Geosci. Model Dev.*,
23 9, 1201–1218, <https://doi.org/10.5194/gmd-9-1201-2016>, 2016.



1 **Table List**

2

3 Table 1. The model experiments with different emissions.

4

5 Table 2. Comparison of the ground-based hourly O₃, NO₂, and CO observations with
6 the simulations utilizing EDGAR-HTAP v2 (EDV2) and v3 (EDV3) and KORUS v5
7 (KOV5) in each regional box (unit = ppb). N is the number of samples. R is correlation
8 coefficient.

9

10 Table 3. Comparison of aircraft-based 1-minute-interval O₃, NO₂, CO, HCHO, TOL,
11 XYL, ETE, and ISO observations with EDV2, EDV3, and KOV5 for all flight cases
12 under 2 km height (unit = ppb). N is the number of samples. R is correlation coefficient.



1 **Figure List**

2

3 Figure 1. The averaged spatial distribution map of the NO, CO, and TOL emissions
4 from EDGAR-HTAP v2, v3, and KORUS v5 in May.

5

6 Figure 2. Averaged O₃ concentrations from ground-based observations and model
7 simulations over the areas that distinguish urban (red box) and non-urban (green box)
8 region (central plot). Box-averaged diurnal cycle (solid lines) of O₃ and 1/4 of standard
9 deviations (filled area) from observations (black), EDV2 (green), EDV3 (blue), and
10 KOV5 (red) by local time are shown. The results are shown for Northern China (NOC,
11 38-42°N/106-110°E), Sichuan-Chongqing-Guizhou (SCG, 27-33°N/103-109°E), Pearl
12 River Delta (PRD, 21.5-24°N/112-115.5°E), Southeastern China (SEC, 24-28°N/116-
13 120°E), Yangtze River Delta (YRD, 30-33°N/119-122°E), South Korea (KOR, 34.5-
14 38°N/126-130°E), North China Plain (NCP, 34-41°N/113-119°E), and Northeastern
15 China (NEC, 43-47°N/124-130°E).

16

17 Figure 3. Comparison of (a) the campaign averaged ground-based maximum daily
18 average of 8-hour O₃ (MDA8 O₃) (unit: ppb) observations and WRF-Chem simulations
19 with (d) EDGAR-HTAP v2 (EDV2), (e) v3 (EDV3), (f) KORUS v5 (KOV5) and (g, h,
20 i) the differences between the observations and model results. The sub-regions are
21 presented with red (urban) and green (non-urban) boxes. The scatter plots comparing
22 averaged observations and the three-emission-based WRF-Chem simulations (green;
23 EDV2, blue; EDV3, red; KOV5) are shown in (b) and (c) for Eastern China and South
24 Korea, respectively. (a, d-e) Color-filled circles in (a), (d), (e), and (f) represent the
25 averaged MDA8 O₃ for the whole campaign period (1st May to 10th June).

26

27 Figure 4. The same as Figure 2 except NO₂.

28

29 Figure 5. The same as Figure 3 except daily NO₂ (unit: ppb).

30

31 Figure 6. The same as Figure 3 except daily CO (unit: ppm).

32

33 Figure 7. The DC-8 flight paths during the KORUS-AQ campaign period (black) and 6
34 regional boxes (1: Seoul Metropolitan Area (SMA); 2: Yellow Sea; 3: Chungnam; 4:
35 Kyungbuk; 5: Gwangju; 6: Busan) (red).

36



1 Figure 8. The mean (bars) and 1/4 of standard deviations (whiskers) of (a) O₃, (b) NO₂,
2 (c) CO, (d) HCHO, (e) TOL, (f) XYL, (g) ethene (ETE), and (h) isoprene (ISO) (unit =
3 ppb) from EDV2 (green), EDV3 (blue), and KOV5 (red) for each box are shown,
4 respectively. TOL and XYL are calculated based on Table S6 (Supporting Information).
5 The contribution of toluene to TOL and m/p-Xylene + o-Xylene to XYL is represented
6 with light grey bars (e, f). The sampling numbers are represented with magenta color
7 above the plots.

8

9 Figure 9. Vertically averaged (a) O₃, (b) NO₂, (c) CO, (d) HCHO, (e) TOL, (f) XYL, (g)
10 ETE, and (h) ISO from DC-8 (black), EDV2 (green), EDV3 (blue), and KOV5 (red) in
11 SMA under 2 km height above ground level. The 1/2 of standard deviations are
12 represented with black whiskers in each 200m layer. The sample number is presented
13 with magenta color on the right side of the plots.

14

15 Figure 10. The diurnal cycles of vertical columns and surface concentrations of (a) NO₂
16 and (b) HCHO from Pandora spectrometer (column), and ground-based instruments
17 (TEI 42i NO_x analyzer and Aerodyne QCL) at the Olympic Park site (37.5232°N,
18 127.126°E). EDV2 (green), EDV3 (blue), and KOV5 (red) are compared with
19 observations. The WRF-Chem vertical column concentrations are produced by
20 summing all vertical layers.

21

22 Figure 11. Diurnal cycles of surface (a) O₃, (b) CO, (c) TOL, and (d) XYL at the
23 Olympic Park site. EDV2 (green), EDV3 (blue), and KOV5 (red) are compared with
24 the observations. 1/4 of standard deviations are represented with grey shades. The
25 average period is from the 11th May to the 10th June.

26

27 Figure 12. Averaged O₃ (bars) and 1/4 of standard deviations (whiskers) (unit: ppbv)
28 for the 20 DC8 flights (under 2 km height). The observations (grey) are compared with
29 the model results utilizing EDV2 (green), EDV3 (blue), and KOV5 (red). White hatch-
30 filled bars over blue bars are the contribution of Chinese emissions to O₃ concentrations
31 obtained from the default and sensitivity model runs with/without Chinese
32 anthropogenic emissions. The Local (5/4,20 and 6/2,3) and Transport (5/25,26,31) cases
33 are shaded with light blue and orange, respectively.

34

35 Figure 13. The biases in (a) the model O₃, (b) CO, and (c) HCHO concentrations (bars)
36 relative to the DC-8 observations under 2 km height over SMA (dark gray: EDV3, red:
37 EDV3 Ch₂, blue: EDV3 ChK_{o2}): (left panel) Local and (right panel) Transport case.
38 Fractional differences (%) are shown in the white boxes.



1 **Table 1.** The model experiments with different emissions

Experiments	Emissions
EDV2	EDGAR-HTAP v2
EDV3	EDGAR-HTAP v3
KOV5	KORUS v5
EDV3_Ch2	EDGAR-HTAP v3 with double CO, VOC emission in China
EDV3_ChKo2	EDGAR-HTAP v3 with double CO, VOC emission in China & South Korea

2



1 **Table 2.** Comparison of the ground-based hourly O₃, NO₂, and CO observations with
 2 the simulations utilizing EDGAR-HTAP v2 (EDV2) and v3 (EDV3) and KORUS v5
 3 (KOV5) in each regional box (unit = ppb). N is the number of samples. R is correlation
 4 coefficient.

Region		¹⁾ NCP	^{1),a)} SCG	¹⁾ YRD	¹⁾ PRD	^{1),b)} KOR (SMA)	^{2),c)} NEC	^{2),d)} NOC	^{2),e)} SEC		
N		190	104	93	68	358 (125)	45	28	43		
O ₃	OBS	Mean	44.5	34.6	38.2	27.9	41.5 (36.6)	40.9	44.3	26.1	
		Mean	32.2	53.5	21.6	27.6	40.5 (31.1)	28.6	39.4	40.8	
	EDV2	Bias	-12.3	18.9	-16.6	-0.3	-1.0 (-5.5)	-12.3	-4.9	14.7	
		R	0.65	0.53	0.62	0.61	0.59 (0.60)	0.48	0.63	0.52	
		Mean	43.4	57.5	35.7	34.7	41.0 (32.6)	35.2	43.7	45.5	
	EDV3	Bias	-1.1	23.0	-2.5	6.8	-0.5 (-4.0)	-5.7	-0.6	19.4	
		R	0.68	0.55	0.66	0.65	0.56 (0.57)	0.63	0.67	0.55	
		Mean	49.0	55.3	41.1	35.7	42.2 (33.1)	37.1	43.8	42.4	
	KOV5	Bias	4.5	20.7	2.8	7.8	0.7 (-3.5)	-3.8	-0.5	16.3	
		R	0.71	0.53	0.65	0.70	0.62 (0.64)	0.62	0.67	0.54	
		Mean	17.5	13.8	17.1	12.9	23.2 (32.5)	13.5	11.9	9.6	
	NO ₂		Mean	25.8	12.7	39.8	22.0	18.8 (29.6)	13.7	12.9	11.0
EDV2		Bias	8.3	-1.0	22.7	9.1	-4.3 (-3.0)	0.2	1.0	1.5	
		R	0.45	0.37	0.38	0.54	0.51 (0.34)	0.49	0.47	0.19	
		Mean	21.8	12.2	30.4	21.0	21.3 (31.8)	11.2	10.3	11.3	
EDV3		Bias	4.3	-1.6	13.3	8.1	-1.9 (-0.8)	-2.3	-1.6	1.7	
		R	0.44	0.34	0.36	0.52	0.49 (0.31)	0.49	0.52	0.22	
		Mean	13.9	7.5	23.5	13.3	17.7 (28.3)	7.0	7.7	7.7	
KOV5		Bias	-3.6	-6.3	6.4	0.3	-5.5 (-4.2)	-6.5	-4.2	-1.9	
		R	0.44	0.37	0.41	0.52	0.51 (0.39)	0.49	0.51	0.26	
		Mean	835	597	694	636	443 (493)	527	579	655	
CO			Mean	373	389	455	282	175 (210)	206	162	258
		EDV2	Bias	-462	-208	-239	-354	-267 (-283)	-321	-417	-397
		R	0.24	0.20	0.42	0.30	0.31 (0.30)	0.21	0.09	0.18	
		Mean	374	359	535	282	196 (208)	221	162	256	
	EDV3	Bias	-461	-238	-159	-354	-247 (-285)	-306	-417	-398	
		R	0.22	0.19	0.35	0.31	0.26 (0.33)	0.24	0.10	0.25	
		Mean	355	358	475	305	190 (217)	231	176	266	
	KOV5	Bias	-480	-239	-219	-331	-253 (-276)	-296	-404	-388	
		R	0.27	0.21	0.48	0.29	0.35 (0.36)	0.15	0.10	0.13	

5 1) Urban area, 2) Non-urban area

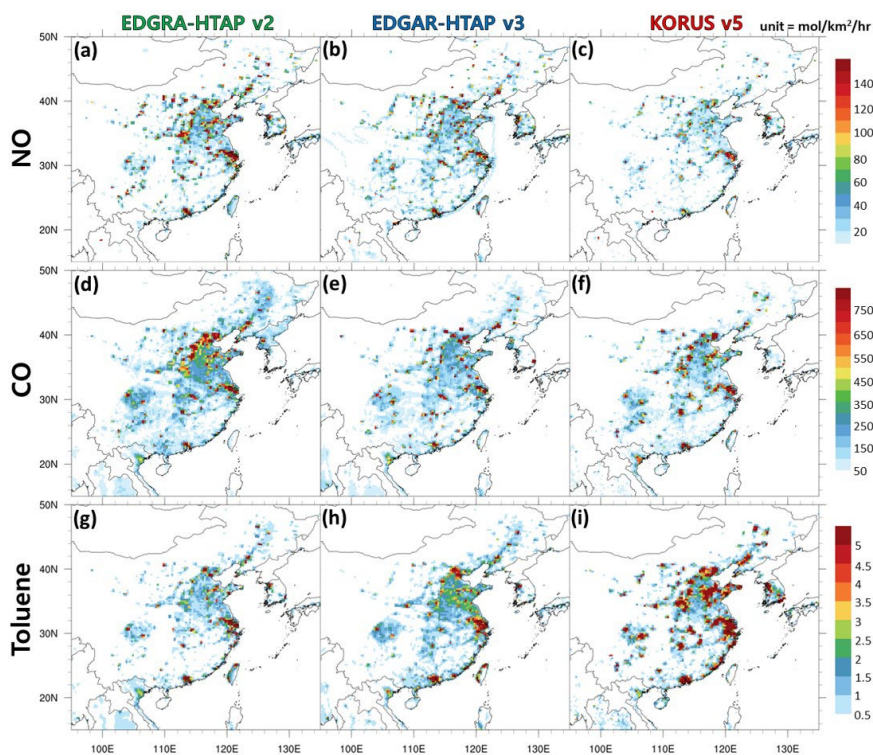
6 a) Sichuan-Chongqing-Guizhou, b) South Korea, c) Northeastern China, d) Northern China, e) Southeastern China



1 **Table 3.** Comparison of aircraft-based 1-minute-interval O₃, NO₂, CO, HCHO, TOL,
 2 XYL, ETE, and ISO observations with EDV2, EDV3, and KOV5 for all flight cases
 3 under 2 km height (unit = ppb). N is the number of samples. R is correlation coefficient.

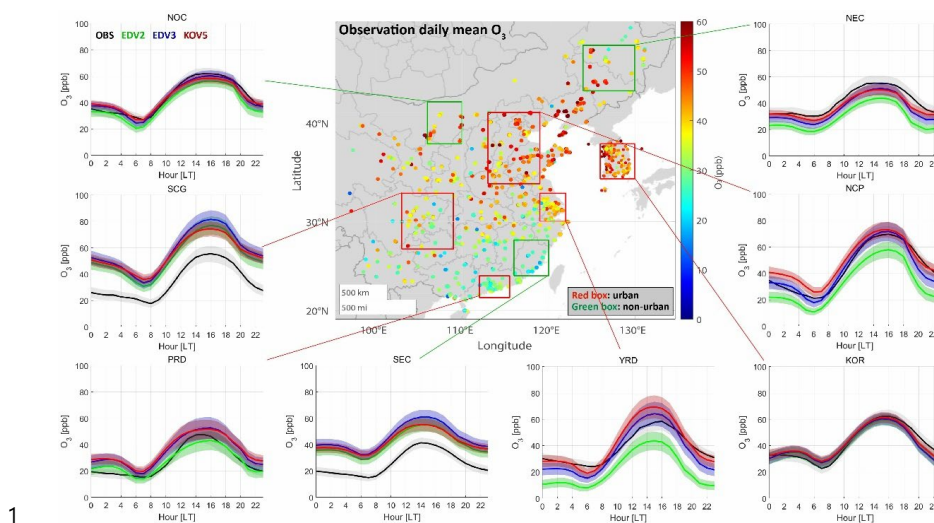
Species	Type	N	Mean	Bias	σ	R
O ₃	OBS	5191	84.4		19.9	
	EDV2		67.5	-16.8	16.7	0.44
	EDV3		69.3	-15.1	17.8	0.43
	KOV5		66.9	-17.5	15.8	0.50
NO ₂	OBS	5047	2.19		4.49	
	EDV2		3.06	0.87	4.60	0.71
	EDV3		3.91	1.72	5.34	0.67
	KOV5		2.83	0.64	4.73	0.73
CO	OBS	5575	253		100	
	EDV2		148	-105	48	0.60
	EDV3		156	-97	47	0.59
	KOV5		146	-107	43	0.62
HCHO	OBS	5365	2.37		1.64	
	EDV2		1.75	-0.62	1.01	0.69
	EDV3		1.78	-0.59	1.02	0.67
	KOV5		1.80	-0.57	1.10	0.71
TOL	OBS	730	2.60		2.02	
	EDV2		0.47	-2.13	0.38	0.39
	EDV3		0.55	-2.05	0.48	0.38
	KOV5		1.58	-1.01	1.30	0.37
XYL	OBS	289	0.73		0.65	
	EDV2		0.23	-0.50	0.23	0.30
	EDV3		0.30	-0.43	0.31	0.30
	KOV5		0.49	-0.24	0.47	0.27
ETE	OBS	2573	0.42		1.59	
	EDV2		0.51	0.09	0.65	0.14
	EDV3		0.56	0.14	0.76	0.15
	KOV5		0.51	0.08	0.58	0.20
ISO	OBS	1294	0.08		0.09	
	EDV2		0.18	0.10	0.21	0.41
	EDV3		0.19	0.11	0.20	0.41
	KOV5		0.17	0.10	0.20	0.42

4

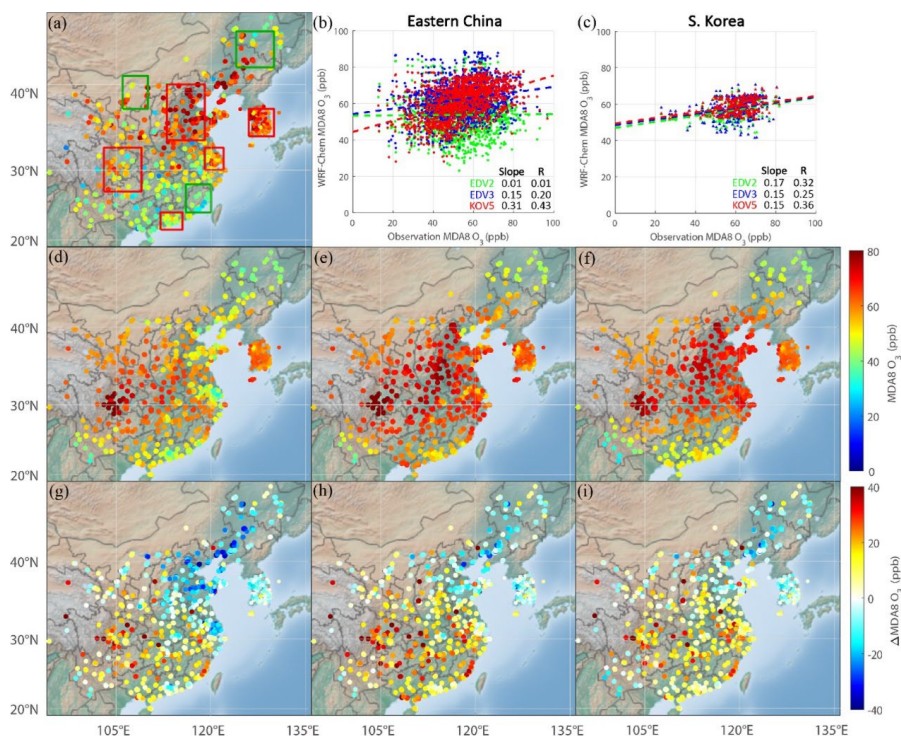


1

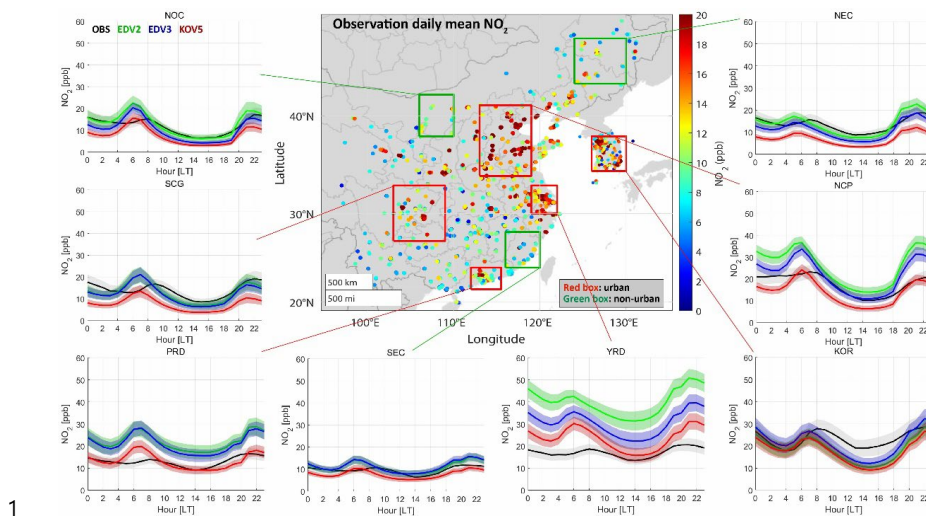
2 **Figure 1.** The averaged spatial distribution map of the NO, CO, and TOL emissions
3 from EDGAR-HTAP v2, v3, and KORUS v5 in May.



1
2 **Figure 2.** Averaged O₃ concentrations from ground-based observations and model
3 simulations over the areas that distinguish urban (red box) and non-urban (green box)
4 region (central plot). Box-averaged diurnal cycle (solid lines) of O₃ and 1/4 of standard
5 deviations (filled area) from observations (black), EDV2 (green), EDV3 (blue), and
6 KOV5 (red) by local time are shown. The results are shown for Northern China (NOC,
7 38–42°N/106–110°E), Sichuan-Chongqing-Guizhou (SCG, 27–33°N/103–109°E), Pearl
8 River Delta (PRD, 21.5–24°N/112–115.5°E), Southeastern China (SEC, 24–28°N/116–
9 120°E), Yangtze River Delta (YRD, 30–33°N/119–122°E), South Korea (KOR, 34.5–
10 38°N/126–130°E), North China Plain (NCP, 34–41°N/113–119°E), and Northeastern
11 China (NEC, 43–47°N/124–130°E).

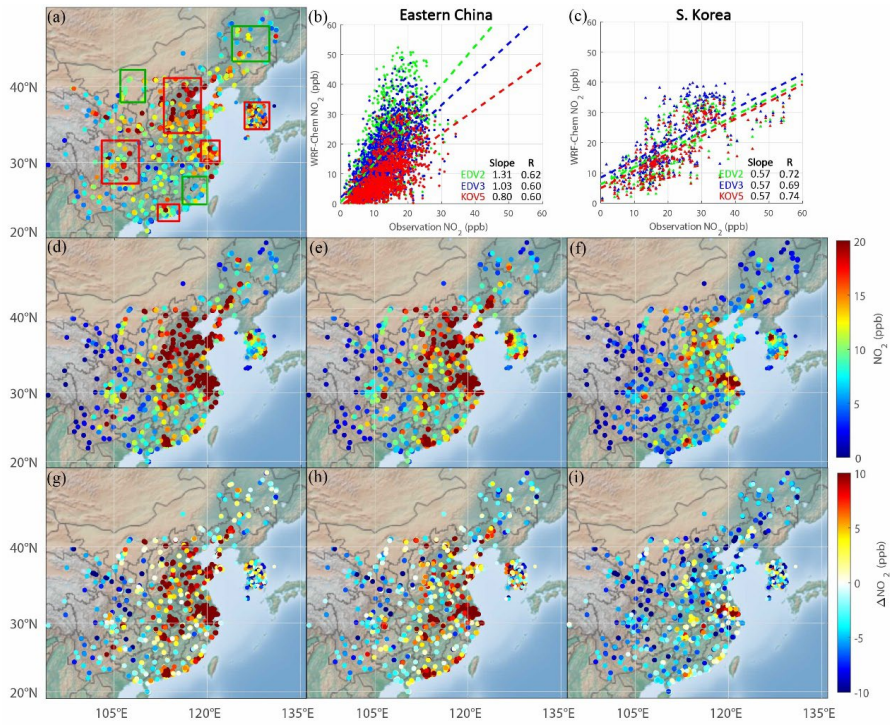


1
 2 **Figure 3.** Comparison of (a) the campaign averaged ground-based maximum daily
 3 average of 8-hour O₃ (MDA8 O₃) (unit: ppb) observations and WRF-Chem simulations
 4 with (d) EDGAR-HTAP v2 (EDV2), (e) v3 (EDV3), (f) KORUS v5 (KOV5) and (g, h,
 5 i) the differences between the observations and model results. The sub-regions are
 6 presented with red (urban) and green (non-urban) boxes. The scatter plots comparing
 7 averaged observations and the three-emission-based WRF-Chem simulations (green;
 8 EDV2, blue; EDV3, red; KOV5) are shown in (b) and (c) for Eastern China and South
 9 Korea, respectively. (a, d-e) Color-filled circles in (a), (d), (e), and (f) represent the
 10 averaged MDA8 O₃ for the whole campaign period (1st May to 10th June).



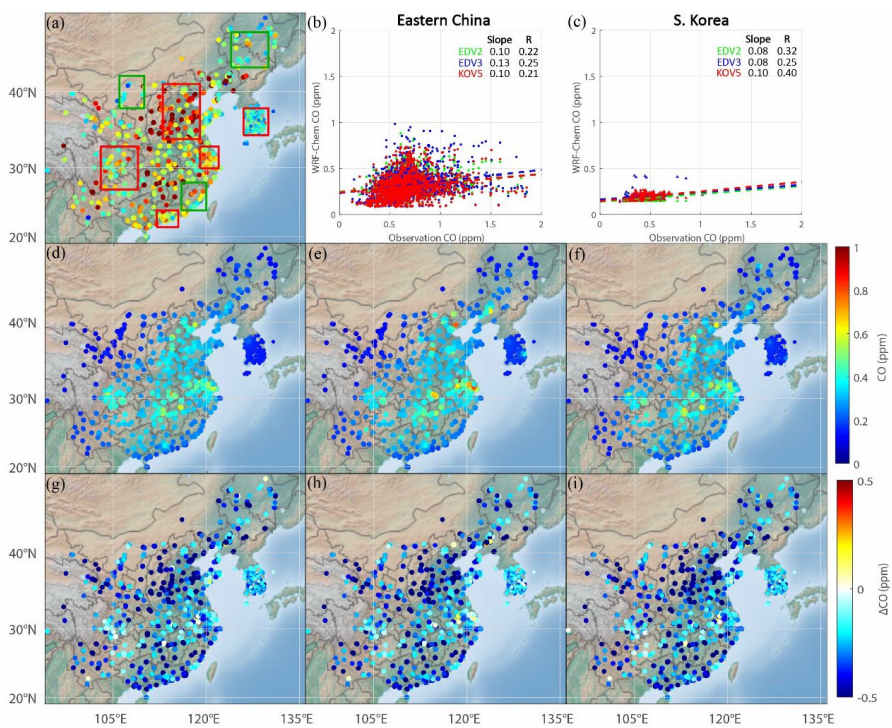
1

2 **Figure 4.** The same as **Figure 2** except NO_2 .



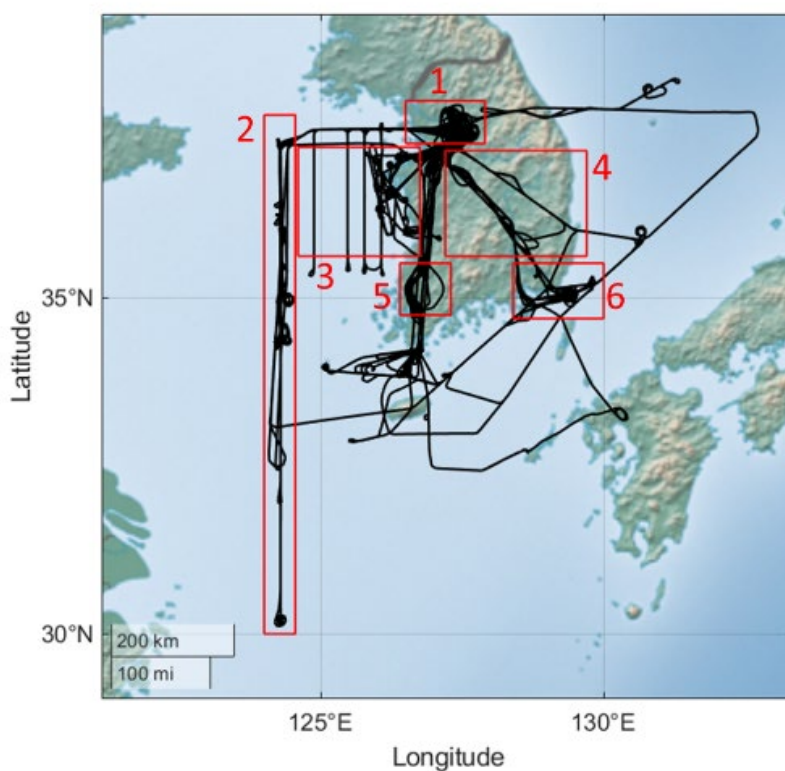
1

2 **Figure 5.** The same as **Figure 3** except daily NO₂ (unit: ppb).

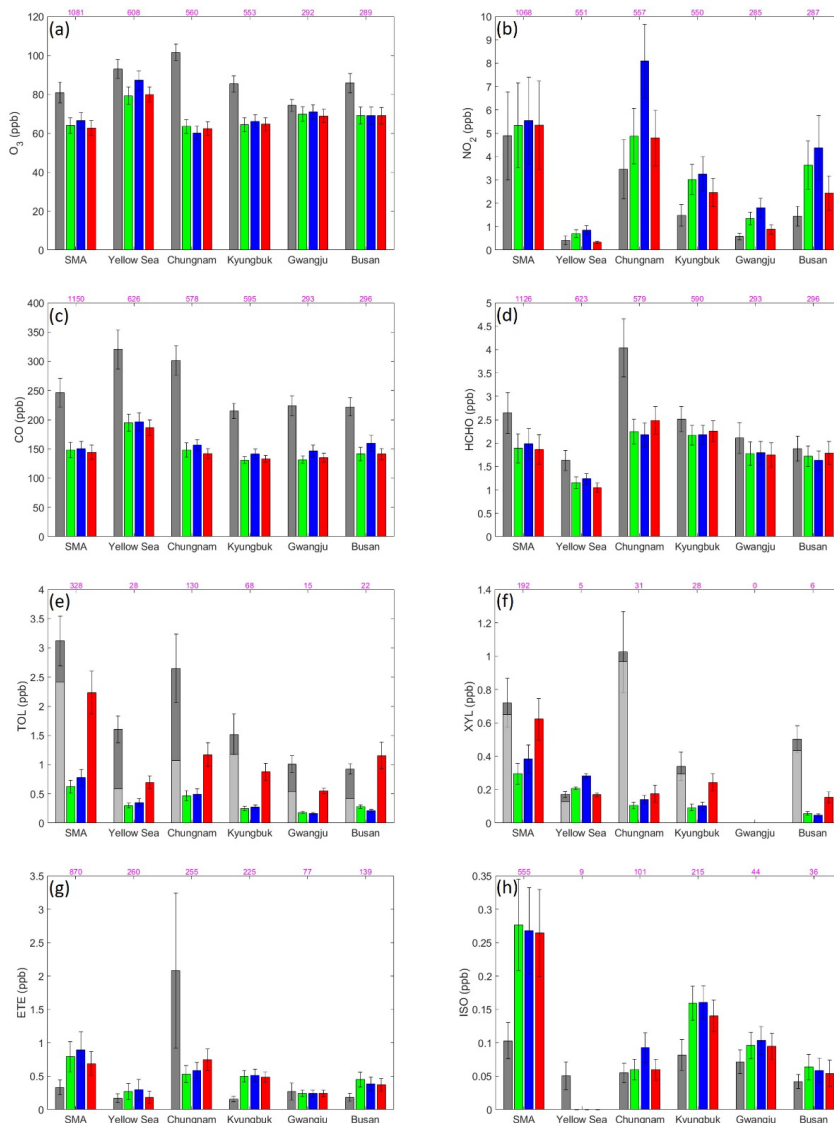


1

2 **Figure 6.** The same as **Figure 3** except daily CO (unit: ppm).

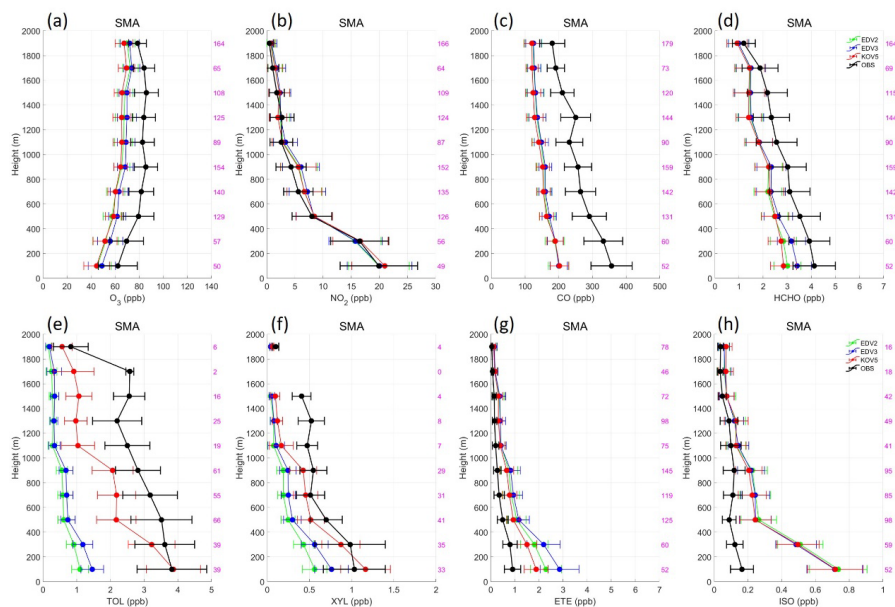


1
2 **Figure 7.** The DC-8 flight paths during the KORUS-AQ campaign period (black) and
3 6 regional boxes (1: Seoul Metropolitan Area (SMA); 2: Yellow Sea; 3: Chungnam; 4:
4 Kyungbuk; 5: Gwangju; 6: Busan) (red).



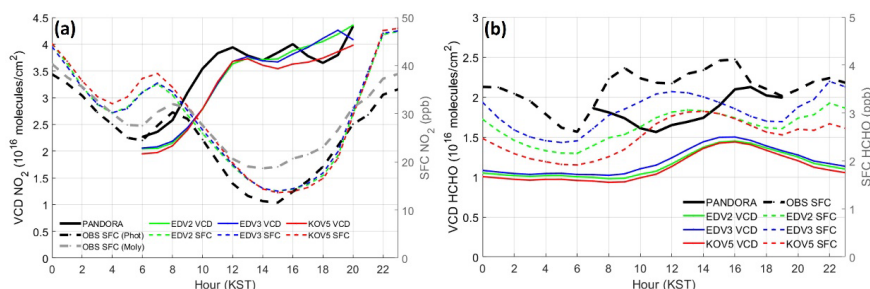
1

2 **Figure 8.** The mean (bars) and 1/4 of standard deviations (whiskers) of (a) O₃, (b) NO₂,
 3 (c) CO, (d) HCHO, (e) TOL, (f) XYL, (g) ethene (ETE), and (h) isoprene (ISO) (unit =
 4 ppb) from EDV2 (green), EDV3 (blue), and KOV5 (red) for each box are shown,
 5 The contribution of toluene to TOL and m/p-Xylene + o-Xylene to XYL is represented
 6 with light grey bars (e, f). The sampling numbers are represented with magenta color
 7 above the plots.
 8



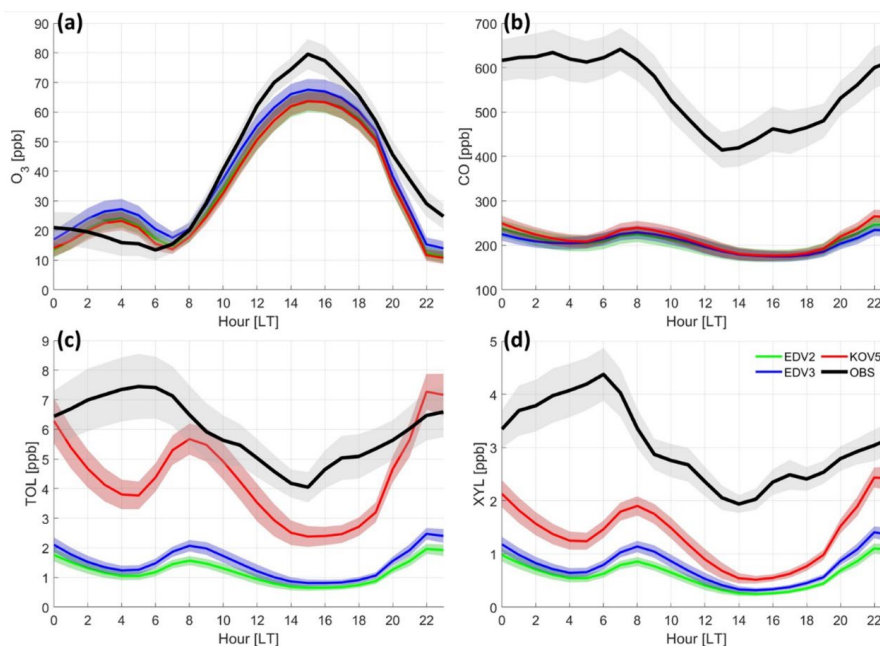
1

2 **Figure 9.** Vertically averaged (a) O₃, (b) NO₂, (c) CO, (d) HCHO, (e) TOL, (f) XYL,
3 (g) ETE, and (h) ISO from DC-8 (black), EDV2 (green), EDV3 (blue), and KOV5 (red)
4 in SMA under 2 km height above ground level. The 1/2 of standard deviations are
5 represented with black whiskers in each 200m layer. The sample number is presented
6 with magenta color on the right side of the plots.



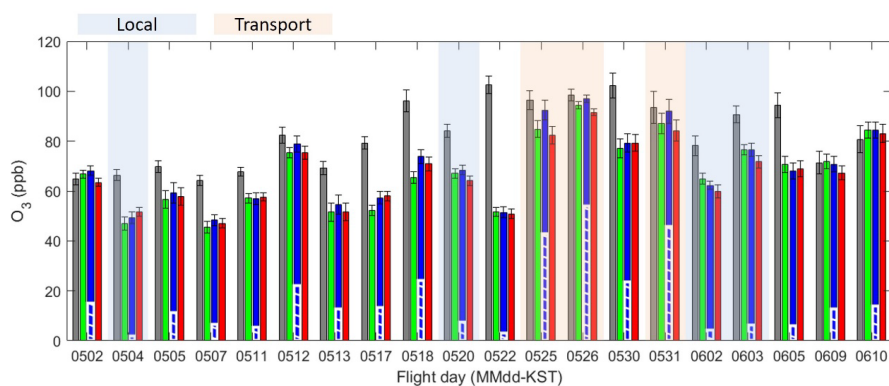
1

2 **Figure 10.** The diurnal cycles of vertical columns and surface concentrations of (a) NO₂
3 and (b) HCHO from Pandora spectrometer (column), and ground-based instruments
4 (TEI 42i NO_x analyzer and Aerodyne QCL) at the Olympic Park site (37.5232°N,
5 127.126°E). Surface concentrations of NO₂ are obtained by the two methods:
6 molybdenum converter and photolytic method. EDV2 (green), EDV3 (blue), and
7 KOV5 (red) are compared with observations. The WRF-Chem vertical column
8 concentrations are produced by summing all vertical layers.



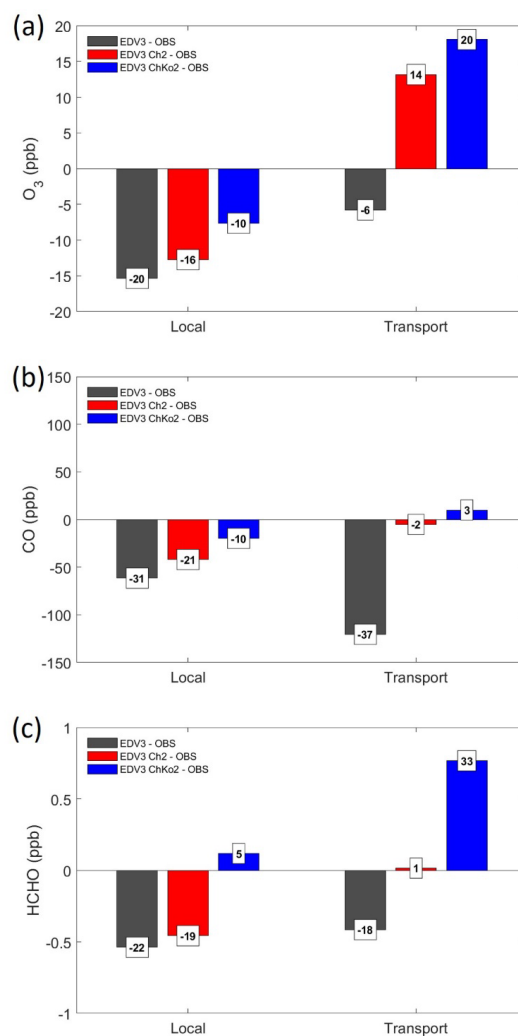
1

2 **Figure 11.** Diurnal cycles of surface (a) O₃, (b) CO, (c) TOL, and (d) XYL at the
3 Olympic Park site. EDV2 (green), EDV3 (blue), and KOV5 (red) are compared with
4 the observations. 1/4 of standard deviations are represented with grey shades. The
5 average period is from the 11th May to the 10th June.



1

2 **Figure 12.** Averaged O₃ (bars) and 1/4 of standard deviations (whiskers) (unit: ppbv)
3 for the 20 DC8 flights (under 2 km height). The observations (grey) are compared with
4 the model results utilizing EDV2 (green), EDV3 (blue), and KOV5 (red). White hatch-
5 filled bars over blue bars are the contribution of Chinese emissions to O₃ concentrations
6 obtained from the default and sensitivity model runs with/without Chinese
7 anthropogenic emissions. The Local (5/4,20 and 6/2,3) and Transport (5/25,26,31) cases
8 are shaded with light blue and orange, respectively.



1

2 **Figure 13.** The biases in (a) the model O₃, (b) CO, and (c) HCHO concentrations (bars)
3 relative to the DC-8 observations under 2 km height over SMA (dark gray: EDV3, red:
4 EDV3 Ch2, blue: EDV3 ChKo2): (left panel) Local and (right panel) Transport case.
5 Fractional differences (%) are shown in the white boxes.